CAPITAL UNIVERSITY OF SCIENCE AND TECHNOLOGY, ISLAMABAD


# Pharmacological Evaluation of Meracaptobenzothiazole Derivative in Animal Models of Alzheimer's Disease

by

Sadia Khaliq

A thesis submitted in partial fulfillment for the degree of Master of Philosophy

in the

Faculty of Pharmacy
Department of Pharmacology

2025

*I dedicate this work*

*To*

*My Beloved Parents and Respected Teachers*

*Who always supplicate for my success, boost my morale and their words are inspirable for me.*

# CERTIFICATE OF APPROVAL

## Pharmacological Evaluation of Meracaptobenzothiazole Derivative in Animal Models of Alzheimer's Disease

by

Sadia Khaliq

(MPH233010)

### THESIS EXAMINING COMMITTEE

| S. No. | Examiner | Name | Organization |
|---|---|---|---|
| (a) | External Examiner | Dr. Salman Khan | QAU, Islamabad |
| (b) | Internal Examiner | Dr. Fazlullah Khan | CUST, Islamabad |
| (c) | Supervisor | Dr. Muzaffar Abbas | CUST, Islamabad |

Dr. Muzaffar Abbas
Thesis Supervisor
August, 2025

Dr. Fazlullah Khan
Head
Department of Pharmacology
August, 2025

Dr. Muzaffar Abbas
Dean
Faculty of Pharmacy
August, 2025

# *Author's Declaration*

I, **Sadia Khaliq** hereby state that my MPhil thesis titled "**Pharmacological Evaluation of Meracaptobenzothiazole Derivative in Animal Models of Alzheimer's Disease**" is my own work and has not been submitted previously by me for taking any degree from Capital University of Science and Technology, Islamabad or anywhere else in the country/abroad.

At any time if my statement is found to be incorrect even after my graduation, the University has the right to withdraw my MPhil Degree.

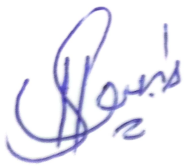

**(Sadia Khaliq)**

Registration No: MPH233010

# *Plagiarism Undertaking*

I solemnly declare that research work presented in this thesis titled "**Pharmacological Evaluation of Meracaptobenzothiazole Derivative in Animal Models of Alzheimer's Disease**" is solely my research work with no significant contribution from any other person. Small contribution/help wherever taken has been duly acknowledged and that complete thesis has been written by me.

I understand the zero tolerance policy of the HEC and Capital University of Science and Technology towards plagiarism. Therefore, I as an author of the above titled thesis declare that no portion of my thesis has been plagiarized and any material used as reference is properly referred/cited.

I undertake that if I am found guilty of any formal plagiarism in the above titled thesis even after award of MPhil Degree, the University reserves the right to withdraw/revoke my MPhil degree and that HEC and the University have the right to publish my name on the HEC/University website on which names of students are placed who submitted plagiarized work.

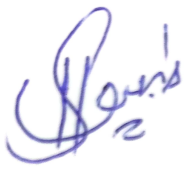

**(Sadia Khaliq)**

Registration No: MPH233010

# *Acknowledgement*

First and foremost, I express my profound gratitude to **Almighty Allah (SWT)**, the source of all strength and wisdom, whose boundless mercy sustained me through the challenges of my M.Phil journey. It is by His grace that I found the resilience to persevere through every obstacle. Peace and blessings be upon **Prophet Muhammad (PBUH)**, whose teachings of compassion, integrity, and pursuit of knowledge have remained a timeless beacon throughout my life.

Firstly, I would like to express my gratitude to Capital University of Science and Technology (CUST) Islamabad for providing me an opportunity to do M.Phil pharmacy and achieving my goal to pursue higher studies. Foremost among them is my esteemed supervisor, **Dr. Muzaffar Abbas** (Dean, Faculty of Pharmacy, Capital University of Science and Technology, Islamabad). His intellectual rigor, visionary guidance, unwavering support and enthusiasm for research transformed my academic journey into an enriching experience. I am indebted to him for opening doors to groundbreaking ideas, securing critical resources, and mentoring me through every obstacle. His ability to weave compelling narratives from complex data not only honed my scientific perspective but also instilled in me a lifelong passion for discovery.

To my seniors, colleagues and lab fellows **Mr. Ibrar Khan, Ms. Aqeela Khurshid, Ms. Iqra Nawaz, Ms. Tuba Naseer, Ms. Iqra Zulfiqar**. Thank you for your technical assistance, valuable collaboration, and moral support. Your presence made the toughest moments more bearable and the successes more meaningful.

I am eternally indebted to my family for their unconditional love and sacrifices. To my parents, whose prayers and unwavering belief in me carried me forward, and to my siblings, **Sumaira Khaliq** and **Humaira Khaliq**, **Mr. Sohaib Khaliq** and **Sayyab Khaliq** thank you for being my strength. Finally, to all those who supported me in ways big and small through kind words, encouragement, or shared

moments of relief thank you. This achievement is not mine alone but the result of collective effort and heartfelt support.

Thank you all once again.

**(Sadia Khaliq)**

# *Abstract*

Alzheimer's disease (AD) is a progressive neurodegenerative disorder characterized by cognitive impairment, synaptic loss, and neuroinflammation. Evidence suggests that increased production of pro-inflammatory cytokines such as tumor necrosis factor-alpha (TNF-$\alpha$) and interleukin-1 beta (IL-1$\beta$) plays a critical role in the pathophysiology of AD. The objective of current study was to investigate the pharmacological effects of 2-(Benzo[d]thiazol-2-ylthio)-n-cyclohexylacetamide, a mercaptobenzothiazole derivative (MBT) and anti-inflammatory agent, in scopolamine-induced AD. The study utilized a multidisciplinary framework, integrating *in vivo* behavioral assessments (Morris water maze and Y-maze tests), biochemical analyses, histopathological evaluation, and *in silico* computational modeling to comprehensively evaluate cognitive function and neuroprotective effects. In behavioral assessments, the MBT significantly enhanced spatial learning and working memory, as demonstrated by a reduction in escape latency and an increase in time spent in the target quadrant in the Morris water maze test, along with a notable rise in spontaneous alternation behavior in the Y-maze test. Moreover, pretreatment with MBT at 10 mg/Kg reduced TNF-$\alpha$ and IL-1$\beta$ expression in mice hippocampus. Taken together, these results suggest that MBT improved memory in scopolamine-induced AD by inhibiting pro-inflammatory signaling pathways. Therefore, MBT could be potential drug candidate for AD with dual anti-inflammatory and neuroprotective effects involving reduced hippocampal TNF-$\alpha$ and IL-1$\beta$ expression and maintaining neuronal integrity.

# Contents

**Author's Declaration** iv

**Plagiarism Undertaking** v

**Acknowledgement** vi

**Abstract** viii

**List of Figures** xii

**List of Tables** xiv

**Abbreviations** xv

**Symbols** xvii

**1 Introduction** 1
- 1.1 Background . . . 1
- 1.2 Etiology of AD . . . 4
  - 1.2.1 Amyloid Hypothesis . . . 6
  - 1.2.2 Tau Hypothesis . . . 6
  - 1.2.3 Mitochondrial Hypothesis . . . 7
  - 1.2.4 Neuroinflammation Hypothesis . . . 8
  - 1.2.5 Cholinergic Hypothesis . . . 8
  - 1.2.6 Oxidative Stress Hypothesis . . . 10

**2 Literature Review** 16
- 2.1 Introduction . . . 16
- 2.2 Cytokines and Immune Signaling in AD . . . 19
- 2.3 Tumor Necrosis Factor-Alpha and Memory . . . 19
- 2.4 Interleukin-1 Beta and Memory . . . 20
- 2.5 Nuclear Factor Kappa B and Memory . . . 22
- 2.6 Neuroinflammation Targeting Therapeutic Strategies for AD . . . 23

**3 Material and Methods** 25
- 3.1 Animals . . . 25
- 3.2 Food Composition . . . 26

3.3 Mice Handling . . . 27
3.4 Mice Bedding . . . 28
3.5 Animal Gender . . . 29
3.6 Randomization . . . 29
3.7 Euthanizing Methods . . . 30
3.7.1 Dislocation . . . 30
3.7.2 Concussion . . . 32
3.8 Chemicals and Drugs . . . 33
3.8.1 Mercaptobenzothiazole Derivative Source . . . 34
3.8.2 Scheme of Synthesis . . . 34
3.9 Acclimatization . . . 35
3.9.1 Grouping of Animals . . . 35
3.9.2 Drug Administration . . . 36
3.9.3 Drug Solubility . . . 37
3.9.4 Dose Preparation . . . 38
3.10 Y-Maze Test . . . 39
3.11 Morris Water-Maze Test . . . 40
3.12 Molecular Docking Studies . . . 42
3.13 Ligand Preparation . . . 42
3.13.1 Protein Preparation . . . 43
3.13.2 Ligand Docking . . . 43
3.13.3 Toxicity Studies . . . 43
3.14 Quantification of Hippocampal Protein Concentration via Bicinchoninic Acid . . . 44
3.15 Determination of Hippocampal IL-1$\beta$ and TNF-$\alpha$ Levels via Sandwich ELISA . . . 46
3.16 Histopathological Evaluation of Hippocampal Tissue using Hematoxylin and Eosin . . . 48
3.17 Statistical Analysis . . . 49

**4 Results** **51**
4.1 Acute Toxicity . . . 51
4.2 Behavioral Assessment . . . 52
4.2.1 Effect of MBT Compound on Spatial Memory Deficit in MWM Test . . . 52
4.2.2 Effect of MBT Compound on Spatial Memory Deficit in Y-Maze Test . . . 54
4.3 Effects of MBT on Proinflammatory Cytokines Expression in Hippocampus of Mice Assessed by ELISA . . . 55
4.3.1 Tumor Necrosis Factor . . . 55
4.3.2 Interleukin-1 Beta . . . 57
4.4 Effects of MBT on Neuronal Survival Assessed by Hematoxylin and Eosin Staining . . . 60
4.5 Molecular Docking Analysis with MBT Compound at Different Cytokines Receptors . . . 61
4.5.1 Tumor Necrosis Factor Alpha . . . 63

4.5.2 Nuclear Factor Kappa . . . . . 65
4.6 In *Silico* Toxicity Studies . . . . . 67

**5 Discussion of Studies** **70**
5.1 In *Vivo* Acute Toxicity Assessment . . . . . 70
5.2 In *Silico* Toxicity Predictions . . . . . 71
5.3 Comparative Behavioral Assessment in Morris Water Maze and Y-Maze Test . . . . . 71
5.4 Comparative Evaluation of MBT on Hippocampal Protein Preservation in Mice . . . . . 73
5.5 Neuroprotective and Anti-Inflammatory Potential of MBT in a Scopolamine-Induced Model of Alzheimer's Disease . . . . . 74

**6 Conclusion and Future Work** **79**
6.1 Conclusion . . . . . 79
6.2 Future Perspectives . . . . . 81
6.3 Limitations . . . . . 82

**Bibliography** **83**

**Appendices** **89**

# List of Figures


1.1 Pathophysiology of Alzheimer's disease (AD). . . . . 2
1.2 Signaling pathway of Alzheimer's disease (AD). . . . . 4
1.3 Major hypothesis involved in pathogenesis of Alzheimer's disease (AD). . . . . 5
1.4 The mitochondrial hypothesis in Alzheimer's disease (AD). . . . . 7
1.5 Major cholinergic projections in central nervous system (CNS). . . . 10
1.6 Role of oxidative stress in progression of Alzheimer's disease (AD). 11

2.1 Mechanism of neuroinflammation in Alzheimer's disease (AD). . . . 21
2.2 Schematic representation of NF-$\kappa$B–mediated neuroinflammation in a scopolamine-induced Alzheimer's disease model. . . . . 22
2.3 Therapeutic strategies of Alzheimer's disease (AD). . . . . 23

3.1 BALB/C mice utilized in study. . . . . 26
3.2 Handling of laboratory mice during experimental procedures. . . . . 27
3.3 Standard housing conditions for laboratory mice. . . . . 28
3.4 Cervical dislocation technique in laboratory mice. . . . . 31
3.5 Synthesis of Benzo[d]thiazol-2-ylthio)-n-cyclohexylacetamide . . . . 34
3.6 Intraperitoneal (i.p.) drug administration in mice. . . . . 37
3.7 Experimental design illustrating the scheme and study plan for scopolamine-induced Alzheimer's disease (AD). . . . . 38
3.8 Y-maze apparatus for spatial learning memory assessment in mice. . 39
3.9 MWM apparatus for assessment of spatial learning and memory in mice. . . . . 41
3.10 Microplate reader thermo scientific multiskan FC. . . . . 46
3.11 Primary coated antibody 96 well plates for ELISA. . . . . 48

4.1 Effects of MBT compound on escape latency in MWM. . . . . 52
4.2 Effects of MBT compound on time spend in target quadrant in MWM. 53
4.3 Effects of MBT compound on % spontaneous alteration in y-maze test. . . . . 54
4.4 Standard curve generated for the quantification TNF-$\alpha$ by using ELISA. . . . . 55
4.5 Effect of treatments on TNF-$\alpha$ level in mice hippocampus measured by ELISA. . . . . 56
4.6 Standard curve generated for the quantification IL-1$\beta$ using ELISA. 57
4.7 Effect of treatments on IL-1$\beta$ levels in mice hippocampus as measured by ELISA. . . . . 58

4.8 Hematoxylin and eosin (H&E) stained coronal sections from the CA1 region of the hippocampus at 10x magnification. . . . . 60
4.9 Toxicity radar chart . . . . . 68

6.1 Graphical summary of MBT neuroprotective effects in an Alzheimer's disease (AD) model. . . . . 80

# List of Tables


3.1 Composition of animal's food . . . . . 26
3.2 Structural Information of Selected Ligands . . . . . 33

4.1 Total protein concentration ($\mu$g/ml) in hippocampus region of mice brain . . . . . 59
4.2 The energy score for the ligand against IL-1$\beta$ . . . . . 62
4.3 The energy score for the ligand against TNF-$\alpha$ . . . . . 63
4.4 The energy score for the ligand against NF-$\kappa$B . . . . . 65
4.5 Molecular interactions of MBT (cyclohexylacetamide) with target inflammatory proteins (IL-1$\beta$, TNF-$\alpha$, and NF-$\kappa$B) based on docking analysis . . . . . 67

# Abbreviations

| | |
|---|---|
| **AChE** | Acetylcholinesterase |
| **AD** | Alzheimer's Disease |
| **ADME** | Absorption, Distribution, Metabolism, and Excretion |
| **APP** | Amyloid Precursor Protein |
| **CNS** | Central Nervous System |
| **DB** | Diagonal Band |
| **GLP** | Good Laboratory Practice |
| **i.p.** | Intraperitoneal |
| **IL-1$\beta$** | Interleukin-1 Beta |
| **IND** | Investigational New Drug |
| **$LD_{50}$** | Median Lethal Dose |
| **MBT** | Mercaptobenzothiazole |
| **MS** | Medial Septum |
| **MWM** | Morris Water Maze |
| **nBM** | Nucleus Basalis of Meynert |
| **NF-$\kappa$B** | B Nuclear Factor kappa |
| **p.o.** | Per Oral |
| **PK** | Pharmacokinetics |
| **ProTox-II** | Predictive Toxicology Tool |
| **ROS** | Reactive Oxygen Species |
| **SAR** | Structure Activity Relationship |
| **SD** | Standard Deviation |
| **SEM** | Standard Error of the Mean |
| **TLR** | Toll-like receptor |
| **TNF-$\alpha$** | Tumor Necrosis Factor-alpha |

**ToxTree** Toxicity Estimation Software

# Symbols

| | |
|---|---|
| **GLP** | Good Laboratory Practice |
| **$\mu$g/ml** | Micrograms per milliliter |
| **mg/Kg** | Milligrams per kilogram |
| **$p < 0.001$** | Very highly significant |
| **$p < 0.01$** | Highly significant |
| **$p < 0.05$** | Statistically significant |

# Chapter 1

# Introduction

## 1.1 Background

Neurodegenerative disorders (NDs) are characterized primarily by the progressive loss of neurons, which is a key pathophysiological alteration in many brain disorders. This deterioration of nerve cells leads to nervous system dysfunction, impacting various functions depending on the affected brain areas [1]. Neurons are essential to the healthy functioning of the human brain because of their vital role in neural transmission. Many neurons are located in the brain however; they can be found elsewhere across the body. Neural stem cells generate the majority of neurons during the early developmental stage, but the process of neurogenesis significantly slows down as one age. Although neurons are not immortal, the continuous irreversible deterioration to their neurons, neuron structure, or their functions, referred as neurodegeneration, is pivotal for number of brain diseases from which most prevalent as AD [2].

Synaptic impairment, disruption of neuronal networks, and the accumulation of abnormally changed protein aggregates within the brain are common features of neurodegeneration. NDs are a collection of disorders most well characterized by neurodegenerative changes include Huntington's disease, prion diseases, amyotrophic lateral sclerosis (ALS), motor neuron disease [3]. Alzheimer's is a neurodegenerative disease that leads to disability in older people. AD, a common type of dementia,

which is diagnosed by increased amyloid beta (A$\beta$), phosphorylated tau protein, and nerve destruction caused by oxidative stress. These parameters change the central cholinergic system and induce unavoidable loss of cognitive function, which worsens memory. Internationally, dementia is a critical public health concern, and its occurrence is on the increase among elderly individuals [4].

Dementia is a clinical syndrome with a marked reduction in cognitive function comprises of memory, language and executive functioning that disables personal activity to accomplish daily task independently to accomplish activities of daily living independently [5]. The World Health Organization estimates that, unless effective prevention strategies are implemented, dementia due to AD would affect 115 million individuals worldwide by 2050. As of today, approximately 6.9 million Americans aged 65 and older suffer from Alzheimer's dementia. In 2060, that figure could reach 13.8 million, unless there are significant medical breakthroughs to prevent or treat the condition [6]. Based on Centers for Disease Control and Prevention statistics, AD is the seventh leading cause of death in the United States in 2022, followed by COVID-19 as the fourth leading cause of death. AD was the sixth most prevalent cause of death, preceded by stroke, before the COVID-19 epidemic. Late-onset AD it typically occurs after 65 years of age. Early-onset AD, occurring before age 65, is less frequent and occurs in about 5% of AD patients [7].

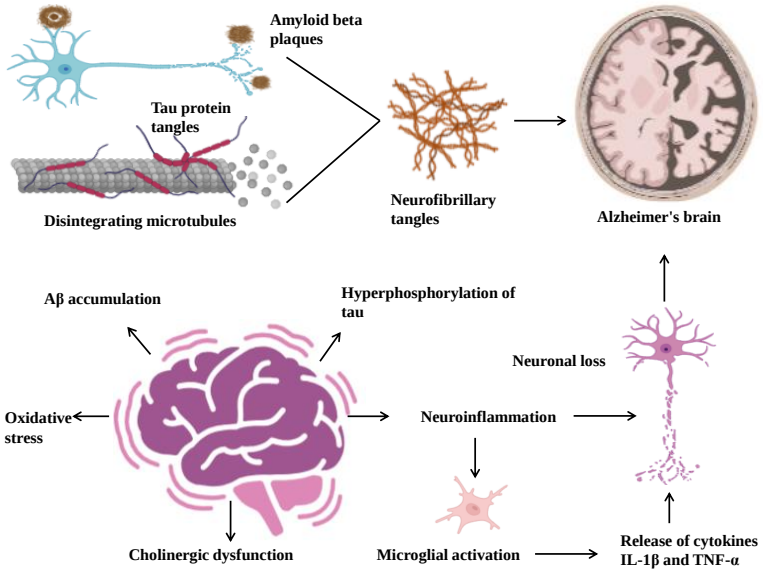


FIGURE 1.1: Pathophysiology of Alzheimer's disease (AD).

The above figure shows extracellular deposition of A$\beta$ peptides, the products of the abnormal cleavage of amyloid precursor protein (APP). The peptides aggregate into amyloid plaques. Their deposition disrupts synaptic transmission, triggers oxidative stress, and causes activation of the brain's resident immune cells, including microglia. Intracellularly, the condition is characterized by the presence of neurofibrillary tangles (NFTs) that consist of hyperphosphorylated tau protein. Under normal circumstances, it helps to stabilize microtubules, but upon hyperphosphorylation, tau loses its function and causes cytoskeletal disintegration as well as axonal transport disruption. As the defective tau proteins form NFTs, they disrupt crucial intracellular functions and cause neuronal death. In addition, activated microglia produce pro-inflammatory cytokines like IL-1$\beta$ and TNF-$\alpha$, adding fuel to neuroinflammation and neuronal damage. These converging pathological processes A$\beta$ deposition, tau pathology, and immune activation eventually lead to progressive synaptic depletion, cortical atrophy, and the cognitive impairment of AD (Figure adopted by Abhijit et.al 2014).

The most common and early symptom in AD is episodic short-term memory impairment. While distant (long-term) memories may initially be reasonably intact, affected people frequently exhibit trouble encoding and remembering new information [8]. Deficits in executive processes, such as judgment, abstract reasoning, problem-solving, and organizing abilities, become noticeable as the illness worsens. The capacity to carry out tasks involving multitasking and higher-order cognitive processes may be severely impacted by these deficiencies. Initially in the disease's progression, instrumental activities of daily life like driving, meal preparation, money management, and intricate planning are usually impaired. [4].

As cognitive decline advances, additional domains become affected. Language disturbances (aphasia) and visuospatial deficits emerge, often followed by a range of neuropsychiatric symptoms. These may include apathy, social withdrawal, disinhibiting, agitation, psychotic features and wandering behaviors, particularly during the moderate to severe stages of AD. Later phases are also marked by extrapyramidal symptoms such dystonia, akathisia, and Parkinsonian characteristics, olfactory dysfunction, disruptions in sleep architecture, and deficiencies in learnt motor tasks

(dyspraxia) [7]. Patients may experience fecal and urine incontinence, primitive reflexes, and complete reliance on caretakers for everyday living activities in the latter stages. The neurodegenerative process that causes AD usually starts in the entorhinal cortex of the hippocampus [9].

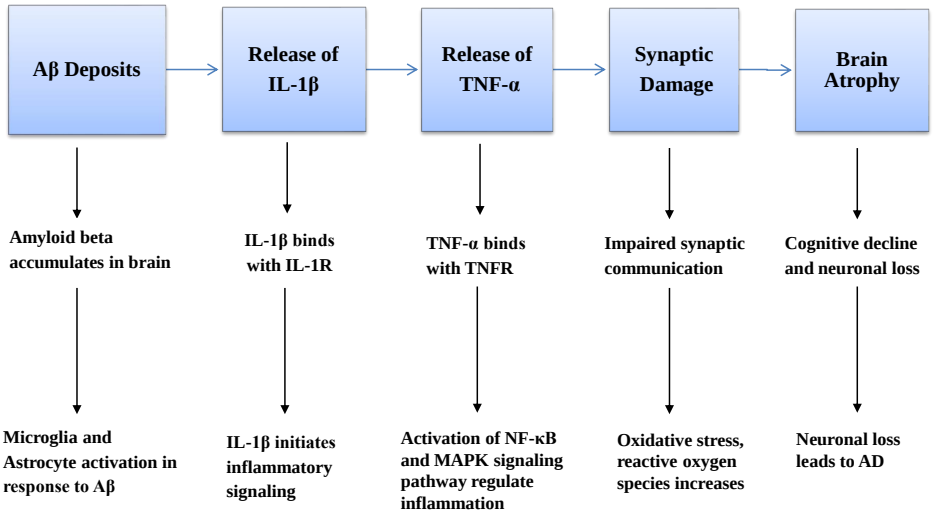


FIGURE 1.2: Signaling pathway of Alzheimer's disease (AD).

The above figure demonstrates that amyloid beta buildup results in the secretion of pro-inflammatory cytokines (IL-1$\beta$ and TNF-$\alpha$), which cause synaptic injury and neuronal apoptosis by mechanisms that include oxidative stress and synaptic stress. A$\beta$ builds up within the brain to become A$\beta$ deposits. This buildup causes the secretion of pro-inflammatory cytokines, such as TNF-$\alpha$ and IL-1$\beta$. IL-1$\beta$ interacts with Interleukin-1 receptor (IL-1R), triggering inflammatory signaling, whereas TNF-$\alpha$ interacts with Tumor necrosis factor receptor (TNFR) and adds to inflammation. Both cytokines result in synaptic harm, deteriorating the communications of the neurons which results in AD (Figure adopted by Kuraishy et.al 2022).

## 1.2 Etiology of AD

Understanding the genesis of AD is crucial for diagnosing and treating the condition yet, despite a variety of possibilities, the true origin of the disease remains unknown

[10]. Amyloid cascade hypothesis is the most accepted hypothesis. In accordance with the amyloid cascade hypothesis, neurodegeneration in AD results from an abnormal deposit of A$\beta$ plaques in different regions of the brain [11].

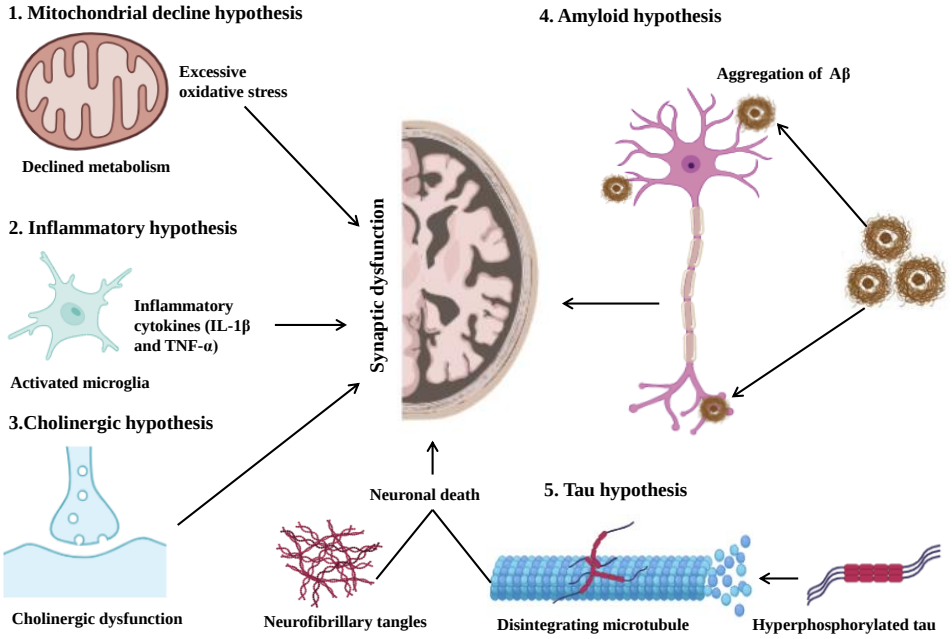


FIGURE 1.3: Major hypothesis involved in pathogenesis of Alzheimer's disease (AD).

The above figure depicts five major scientific hypotheses include the mitochondrial decline hypothesis suggests that when the mitochondria become damaged, they produce harmful oxidative stress and reduce the cell's energy supply. This damages brain cells and affects their ability to communicate properly. The inflammatory hypothesis provides that in AD, the immune cells of the brain, (microglia) become hyperactive and secrete inflammatory chemicals such as IL-1$\beta$ and TNF-$\alpha$. These chemicals kill neurons and interfere with the communication between neurons. The cholinergic hypothesis is concerned with the degeneration of cholinergic neurons, which synthesize acetylcholine, a chemical necessary for memory and learning. When these neurons are injured, problems with memory occur and abnormal shapes such as neurofibrillary tangles start to develop. Alzheimer's disease resulting from the deposition of amyloid-beta (A$\beta$) proteins outside of neurons based on the amyloid hypothesis. These clumps become plaques that block communications between brain cells and cause toxic effects in the brain. Lastly, the tau hypothesis explains

how one of the proteins known as tau becomes abnormally hyperphosphorylated, leading it to detach from microtubules (which support the structure of the cell). This results in breakdown of microtubules and tangle formation within neurons, ultimately leading to their death. All these mechanisms play a role in synaptic dysfunction and eventually result in neuronal death, which are the hallmark characteristics observed in the brains of AD patients (Figure adopted by Wael et.al 2022).

### 1.2.1 Amyloid Hypothesis

The primarily caused of AD is the peptide A$\beta$, which is produced when the transmembrane amyloid precursor protein (APP) is broken down by proteases. A$\beta$ deposition and aggregation in the brain are early and crucial processes that result in neuronal dysfunction and are a hallmark of AD. A$\beta$ peptides of different lengths can be produced by $\gamma$-secretase cleaving APP at several locations, the most common isoforms are amyloid-$\beta$40 and amyloid-$\beta$42 (A$\beta$42). Among these, A$\beta$42 is more likely to aggregate and has a higher neurotoxicity level. It primarily builds up in brain lesions. Although A$\beta$40 is generated in the peripheral and CNS, it is also associated to a number of cardiovascular diseases. However, new research suggests that it also builds up in the bloodstream, arterial walls, and cardiac tissues [12]. Additionally, accumulated A$\beta$ amyloid results in neurodegeneration and neuronal cell death.

### 1.2.2 Tau Hypothesis

The tau hypothesis holds that one of the primary causative elements in the pathophysiology of AD is abnormal accumulation of tau protein in the brain. Microtubules are essential to maintaining neuronal structure and facilitating intracellular passage of nutrients and signaling molecules. Tau is an essential microtubule-associated protein that stabilizes microtubules in normal physiological conditions. Abnormal tau modifications result in its aggregation as NFTs in AD. Cognitive loss is further promoted by these tangles due to the fact that they induce microtubule instability,

interfere with neuronal transport pathways, and finally result in neuronal dysfunction and death. Therefore, a lot of current research focuses on the development of therapeutics that will prevent tau aggregation or induce clearance of tau from the brain. Upon detachment from microtubules, tau proteins disrupt intracellular transport, leading to neuronal dysfunction and reduced activity in the brain. It can even lead to macroscopic brain atrophy and death. Intracellular tangles interfere with axonal transport as well as synaptic signaling and hence ultimately lead to neuronal dysfunction and death [13].

### 1.2.3 Mitochondrial Hypothesis

It is well acknowledged that in the brains of Alzheimer's patients, mitochondrial activity is disturbed, and that NPs (Neuritic plaques) collect within mitochondria. But it's unknown if mitochondrial dysfunction causes or results from NP aggregation. The mitochondrial cascade hypothesis was proposed in response to these problems [14].

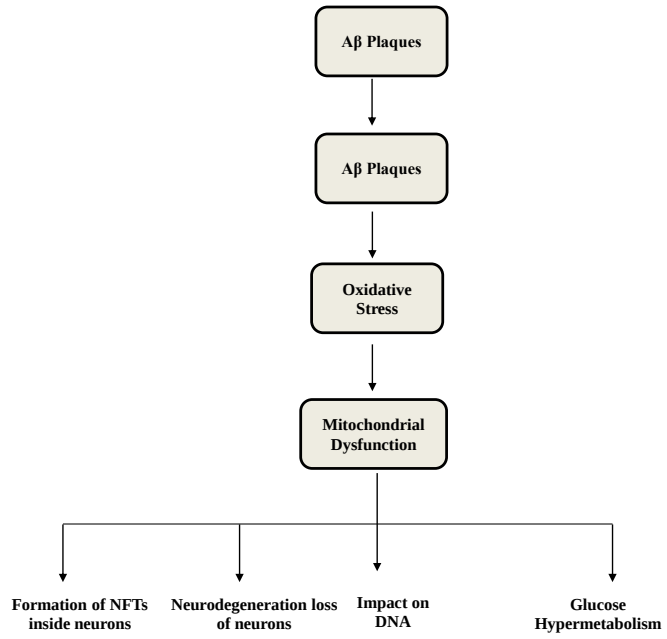


FIGURE 1.4: The mitochondrial hypothesis in Alzheimer's disease (AD).

The above figure describes the abnormal accumulation of A$\beta$ peptides that initiates oxidative stress and mitochondrial dysfunction, resulting in mitochondrial

fragmentation, impaired mitophagy, and disrupted axonal transport. These events compromise neuronal energy metabolism, alter mitochondrial DNA methylation, and contribute to synaptic failure and tau pathology. Collectively, these mitochondrial impairments are proposed to drive neurodegeneration and cognitive decline in AD (Figure adopted by Rishika et.al 2022).

### 1.2.4 Neuroinflammation Hypothesis

The inflammation hypothesis highlights the central role of chronic neuroinflammation in the pathogenesis and development of AD. Neuronal injury and cognitive impairment in patients with AD have been correlated with increased levels of inflammatory mediators, including cytokines and chemokines. Microglia, the central nervous system's resident immune cells, play a dual role in AD. Under physiological conditions, they maintain homeostasis by clearing debris and misfolded proteins, and in early AD stages, they may exert neuroprotective effects by phagocytosing amyloid-beta (A$\beta$) and tau aggregates. However, as the disease advances, persistent exposure to elevated A$\beta$, hyperphosphorylated tau, and damage-associated molecular patterns leads to chronic microglial activation.

Overactivated microglia release excessive pro-inflammatory cytokines, chemokines, and reactive oxygen species, exacerbating neuronal injury and promoting neurodegeneration. This shift from protective to pathogenic activity highlights the complexity of microglial involvement in AD. Lipids, proteins, and DNA structures can all be harmed by this process. The development of AD would result from a decline in antioxidant levels brought on by an increase in apoptosis and mitochondrial malfunction [15].

### 1.2.5 Cholinergic Hypothesis

Based on the cholinergic hypothesis, in the 1970s, studies found that AD subjects suffered from cognitive breakdown as a consequence of a reduction in cholinergic neurons and depletion of choline acetyltransferase, a synthetic enzyme for ACh, in

the cortex and hippocampus. The cholinergic neurons send projections along the CNS. Two large cholinergic projection subsystems can be characterized. The first cholinergic system emerges in the basal forebrain and makes diffuse projections primarily over cortex and hippocampus. The second prominent cholinergic system emerges from pedunculopontine tegmentum and laterodorsally pontine tegmentum neurons. It sends widespread descending innervation to the brain stem. It also provides ascending innervation primarily to the thalamus and midbrain regions, such as the dopaminergic neurons of the substantia nigra and ventral tegmental area.

The cholinergic neurotransmission system of the brain is one of the major channels of memory and cognition. The principal roles of ACh are synaptic transmission at the neuromuscular junction, synaptic plasticity, attention, stress response, learning and memory. The A$\beta$ peptides accumulate in the cholinergic neurons where they are transported inside mitochondria and suppress the activity of pyruvate dehydrogenase, a vital enzyme that generates acetyl-CoA. This disruption is detrimental to the synthesis of ACh, a neurotransmitter necessary for cognitive activity. In advanced AD, there is a significant reduction in expression of choline acetyltransferase (ChAT) and the activity of acetylcholinesterase (AChE), indicating extensive decline in cholinergic neuronal function [16]. Additionally, there is a pronounced reduction in the density of both nicotinic and muscarinic acetylcholine receptors across key brain regions such as the cortex, hippocampus, and basal forebrain. Among these, the $\alpha$7 nicotinic acetylcholine receptor (nAChR) plays a pivotal role by mediating the internalization of A$\beta$ peptides. Its high expression in the neocortex, thalamus, striatum, and hippocampus underscores its involvement in age-related cognitive decline. The accumulation of amyloid plaques further disrupts critical neuronal processes including memory formation, synaptic plasticity, and excitability ultimately impairing the ability of muscarinic receptors to propagate cholinergic signals. Cholinergic activity significantly decreased, which is the initial pathophysiological component associated with AD. ACh production or presynaptic recapture changes in conjunction with neurodegeneration of cholinergic neurons, leading to a progressive loss of memory capacity. Because of this evidence, a cholinergic hypothesis of the disease has been developed as a research platform to

uncover long-term solutions for cholinergic impairments; this will help AD patients regain their memory function [18].

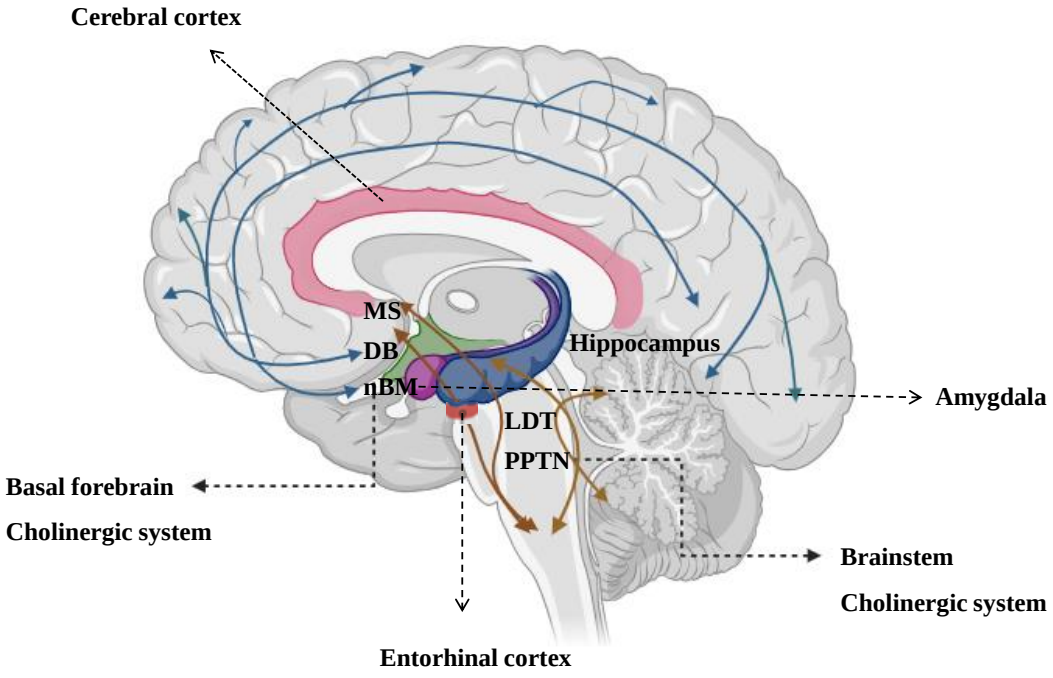


FIGURE 1.5: Major cholinergic projections in central nervous system (CNS).

The above figure demonstrates the basal forebrain cholinergic system which includes the medial septum (MS), diagonal band of broca (DB), and nucleus basalis of Meynert (nBM) projecting primarily to the hippocampus and cortex. Additionally, the brainstem cholinergic system, composed of the laterodorsal tegmental nucleus (LDT) and pedunculopontine tegmental nucleus (PPTN), projects to various subcortical and cortical regions (Figure adopted by Newman et.al 2012).

### 1.2.6 Oxidative Stress Hypothesis

Oxidative stress hypothesis holds that the brain tissue of subjects with AD undergoes enormous oxidative stress as the disease advances. Oxidative stress, described as a discrepancy between the excess production of reactive oxygen species (ROS) and poor antioxidant defense system, is established to play an important role in age-associated neurodegeneration and cognitive impairment [17].

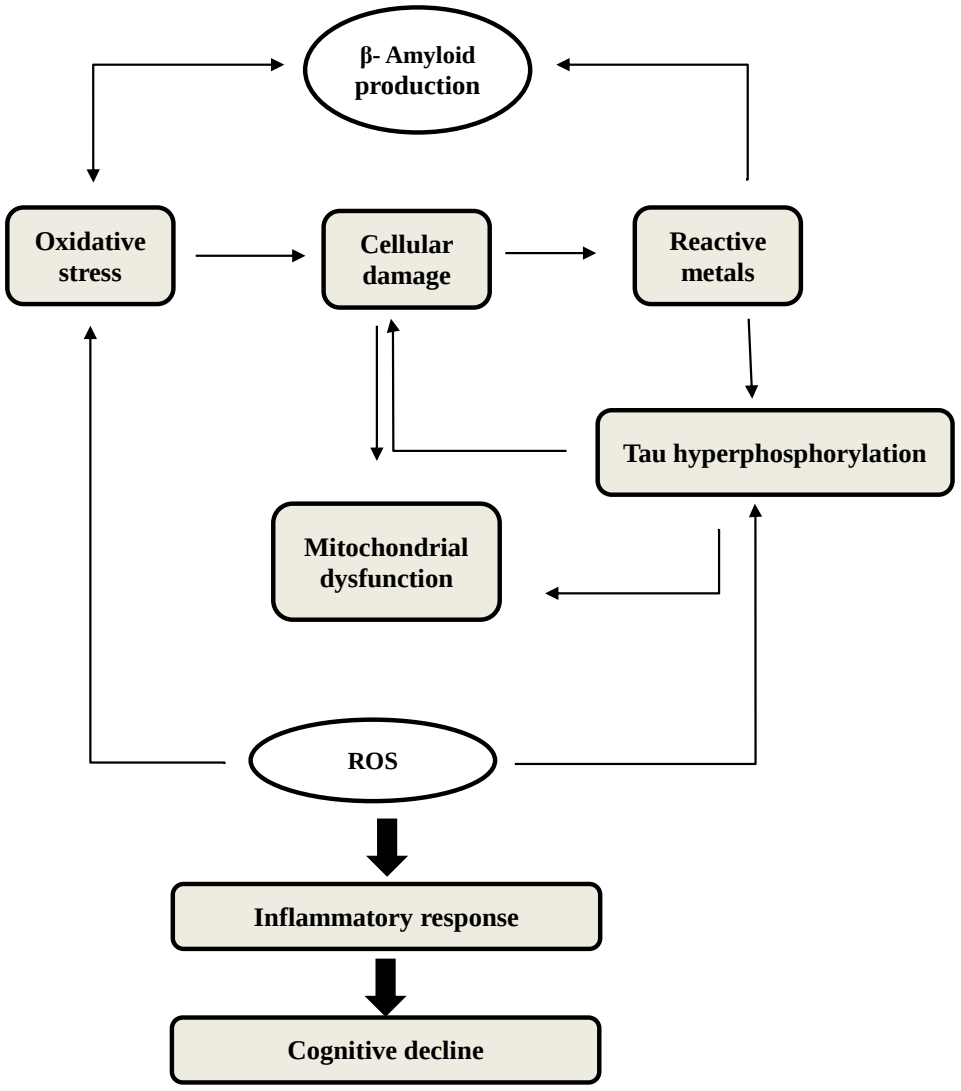


FIGURE 1.6: Role of oxidative stress in progression of Alzheimer's disease (AD).

The above figure shows key pathological initiates that disturb various cellular processes such as mitochondrial function, membrane integrity, and antioxidant defense. It induces inflammation, metal ion imbalance, and synaptic dysfunction, and also A$\beta$ accumulation and tau tangle formation. The accumulating oxidative stress may lead, to trigger cellular dysfunction, inflammatory reactions and cognitive impairment (Figure adopted by Olivier et.al 2011).

Each of above possibility is likely to have both genetic and nongenetic determinants Advanced age is the most important risk factor for AD, with prevalence doubling every five years from the age of 65. Of the modifiable risk factors, cardiovascular

diseases (CVD) are particularly important. CVD not only contributes to the risk of AD development but also to other dementias, like vascular dementia, via mechanisms like stroke and compromised cerebral perfusion. As a result, CVD is increasingly recognized as a modifiable risk factor for AD pathogenesis [18].

Early symptoms of AD in patients, include behavioral abnormalities, cognitive decline, and memory impairment. AD's clinical course can be roughly divided into multiple phases according to the degree of symptoms and underlying neuropathological alterations [18]. The initial stage, referred to as the preclinical or presymptomatic stage, can last for a number of years and is distinguished by minor memory impairments and other subtle cognitive changes without any functional impairment that are clinically evident. Although people at this stage are still functionally independent and do not exhibit any overt clinical symptoms of dementia, they are distinguished neuropathologically by the early accumulation of amyloid-beta plaques and NFTs in areas like the cerebral cortex and hippocampus.

As the disease advances into the mild or early symptomatic stage, patients begin to exhibit noticeable deficits that interfere with everyday functioning. These include impaired memory, reduced attention and concentration, temporal and spatial disorientation, mood disturbances, and in some cases, the emergence of depressive symptoms. The ability to perform routine daily activities gradually declines during this phase [19].

In the moderate stage of AD, pathological changes extend to larger areas of the cerebral cortex, resulting in more pronounced cognitive and functional impairments. Individuals often experience substantial memory loss, including difficulty recognizing familiar people such as family and friends. Language deficits, including problems with reading, writing, and speaking, become evident, along with behavioral symptoms such as irritability, agitation, and impaired judgment or impulse control [20].

The severe or late stage of AD is characterized by extensive cortical damage with widespread deposition of neuritic plaques and NFTs. Patients in this stage suffer from profound cognitive deterioration and are typically unable to recognize

close relatives or engage in meaningful communication. Functional dependence becomes total, as individuals lose the ability to walk, eat, or perform basic self-care tasks. Complications such as dysphagia, urinary incontinence, and immobility are common, often leading to life-threatening conditions and ultimately resulting in death.

Brain regions involved in AD include hippocampus, entorhinal cortex, and neocortex regions these are crucial for memory and cognition impairment. The hippocampus, a bilateral structure situated within the medial temporal lobe, plays an essential role in consolidating short-term memories into long-term storage and supports spatial learning and cognitive functions. In AD, the hippocampus is among the earliest and most profoundly affected regions, exhibiting progressive neuronal degeneration and atrophy. This degeneration is driven by the accumulation of amyloid-beta (A$\beta$) plaques and neurofibrillary tangles (NFTs) composed of hyperphosphorylated tau protein. These pathological features are predominantly concentrated in the hippocampal region, where they contribute to synaptic disruption, mitochondrial dysfunction, oxidative stress, and neuroinflammation. These cellular and molecular disturbances impair neuronal function and connectivity, ultimately leading to the memory loss and cognitive decline that characterize the clinical presentation of AD [21].

During normal aging, the brain undergoes a modest degree of shrinkage; however, significant neuronal loss is not typically observed. In AD, by contrast, widespread neurodegeneration occurs. Many neurons become impaired, lose their synaptic connections, and eventually die. The disease interferes with essential neuronal functions, including communication, energy metabolism, and cellular repair mechanisms.

During the initial stages of AD, it mostly targets synaptic linkages in brain areas essential for memory, including the hippocampus and entorhinal cortex. With progressing disease, other areas of the cerebral cortex responsible for language, reasoning, and social behavior are targeted [22]. The FDA has only licensed a few number potential therapeutic strategies for AD include cholinesterase inhibitors (donepezil, rivastigmine, galantamine, tacrine), NMDA receptor antagonist

(memantine), and amyloid-targeting therapies like monoclonal antibodies (aducanumab) and BACE inhibitors [23]. Tau-targeting therapies aim to prevent tau aggregation. Anti-inflammatory drugs, lifestyle interventions (omega-3-rich diets), neuroprotective agents (antioxidants), gene therapy, and stem cell therapy has also been explored. Combination therapies integrating multiple approaches offer synergistic benefits for treating AD symptoms and pathology. These medications function by raising the brain's ACh level. However, because these medications have severe adverse effects such hepatotoxicity, their effectiveness is restricted [24].

Advanced treatments like monoclonal antibodies show promise but also face challenges, including high costs and the need for more extensive clinical validation [25]. These findings highlight potential avenues for preventive interventions that could reduce the risk of AD-related cognitive decline and may also have broader implications for neurodegenerative diseases in general. A major challenge in the field remains the enhancement of early detection methods, particularly during the preclinical phase of the disease prior to the onset of noticeable symptoms when therapeutic intervention is likely to be most effective [26].

The effective distribution and targeted transport of therapeutic drugs to the brain remains a key issue in the development of viable therapeutics for AD, mostly because of central nervous system (CNS) protective barriers. One of the primary obstacles is the blood-brain barrier (BBB), a highly selective and tightly regulated interface that serves to protect the brain from harmful substances such as neurotoxins, pathogens, and circulating chemicals. While the BBB is crucial for maintaining CNS homeostasis, it also presents a major limitation by restricting the entry of many potentially beneficial therapeutic molecules, thereby hindering effective drug delivery to the target neural tissue [27].

Existing treatment modalities are inadequate, providing only symptomatic relief for a limited duration without stopping disease progression. Research is subsequently being directed toward finding cholinesterase inhibitors that are capable of enhancing the activity of ACh, anti-amyloid drugs, employment of anti-oxidants, and anti-inflammatory medication. The creation of cholinesterase inhibitors, capable of enhancing the activity of ACh, anti-amyloid drugs, and antioxidants, as well

as anti-inflammatory medications, is the area of emphasis in existing research. The difficulties of early diagnosis, efficient drug delivery through the BBB, and the multi-factorial etiology of AD pathology highlight the imperative for new, disease-modifying treatments.

As the current treatments are limited and the incidence of AD continues to rise, there is a critical need to discover new therapeutic targets that can act at early stages of pathogenesis. Research into the cholinergic system, amyloid and tau pathways, neuroinflammatory processes, and oxidative stress-mediated damage provides an integrated platform for building effective therapies. This highlights the importance of ongoing research in early diagnosis, enhanced drug delivery systems, and discovery of new neuroprotective agents.

An organosulfur heterocyclic molecule with a fused benzene and thiazole ring system is called mercaptobenzothiazole (MBT). It is widely known to have anti-inflammatory effects, which are mainly achieved via modifying oxidative stress pathways and inhibiting pro-inflammatory cytokines. The current study used molecular docking analyses to assess three MBT derivatives: octylamine, morpholine, and cyclohexylactamide. When compared to the other derivatives, the Cyclohexylactamide derivative showed the highest binding affinity, suggesting a better interaction with the target site. Numerous biological actions, such as antitubercular, anti-inflammatory, anticancer, antiamoebic, antiparkinsonian, anthelmintic, antihypertensive, antihyperlipidemic, antiulcer, chemoprotective, and selective CCR3 receptor antagonist qualities, have been demonstrated by this chemical [28].

# Chapter 2

# Literature Review

## 2.1 Introduction

AD is a progressive neurodegenerative disease first reported by Alois Alzheimer in 1906. It is characterized by memory impairment, cognitive function reduction, and significant neuropathological changes in the brain. A leading cause of dementia, AD raises an important and growing public health issue, particularly as the global population ages. The connection between neuroinflammation and AD is understood when one considers the phenomenon of inflammaging as a process of chronic, low-grade inflammation associated with aging. Aging per se is a main risk factor for AD, and inflammaging adds to the neuroinflammatory environment through increased levels of reactive oxygen and nitrogen species. These free radicals disturb intracellular signaling, induce cellular senescence, and cause pyroptotic cell death. These cumulative molecular activities compromise the structural and functional integrity of the BBB, further enabling peripheral immune components to invade the CNS and enhance inflammation [29]. The concept of the CNS as an "immune-privileged" site has been recognized since the 1960s, first introduced by Sir Peter Medawar and Sir Frank Macfarlane Burnet on the grounds that the BBB allowed full insulation of the brain from the peripheral immune system [9]. This was the basis for early hypotheses of neurodegenerative disease pathophysiology, in which inflammation was not regarded as a primary factor. Yet, cumulative evidence over the last decades has countered this view. It is now firmly established that the BBB is not a

solid wall but a dynamic and selectively permeable interface that can become breached in both aging and disease. Cytokines and other inflammatory mediators can affect BBB permeability, promote the infiltration of immune cells and create a connection between peripheral inflammation and central neurodegeneration [30].

This developing awareness is especially important in the case of AD where neuroinflammation is being identified as an integral part of pathogenesis with greater and greater recognition. Instead of being an effect of neuronal loss, inflammation in AD frequently is a precursor to and a promoter of the pathological cascade including A$\beta$ deposition, tau phosphorylation, synaptic impairment, and neuronal loss. Activated microglia, the brain's resident immune cells, have a two-pronged role. First, they try to eliminate A$\beta$ deposits and restore homeostasis, but repeated activation results in the release of pro-inflammatory cytokines and neurotoxic products that reinforce the cycle of neurodegeneration [31].

Nonetheless, BBB impairment in aging and AD particularly within the hippocampus allows complement components to be deposited adjacent to A$\beta$ plaques and tau tangles. This not only indicates continued immune activation but also implies a function for complement both in clearance and damage. For instance, C3a/C3aR signaling has been shown to disrupt vascular endothelial cadherin junctions, compromising barrier integrity[32].Interestingly, C3aR1 inhibition has been found to decrease microglial activation and normalize cortical and hippocampal volume, demonstrating the promise of the modulation of complement signaling to dampen neuroinflammation and neurodegeneration [23].

In spite of the established role of inflammation in AD, therapeutic efforts to downregulate is most notably with the use of non-steroidal anti-inflammatory drugs (NSAIDs) have been disappointing. While epidemiological evidence supports long-term NSAID use as lowering AD risk, clinical trials of symptomatic patients have been unsuccessful at proving efficacy. These failures are probable due to more than one factor, as interventions are too late, suboptimal dosing regimens, and incomplete appreciation of the dual role of inflammation. The majority of available anti-inflammatory agents suppress pro-inflammatory processes without triggering anti-inflammatory or reparative mechanisms [33]. This reflects a key paradigm shift, instead of generally dampening inflammation,

emerging approaches must target specific inflammatory processes amping beneficial responses while quelling harmful ones.

Another challenge of equal significance is early detection and monitoring of neuroinflammation. The absence of adequate CNS-specific inflammatory biomarkers currently holds up timely diagnosis and therapy. Peripheral markers, however, including serum and plasma cytokines that reflect corresponding CNS inflammation, are actively under investigation. These can potentially function as readily accessible, non-invasive markers of disease onset and progression, especially when combined with neuroimaging and cognitive measures. Development of these biomarkers will not just help in early detection but will also facilitate patient stratification for individualized immunotherapeutic interventions [34].

Lastly, the complex interface between CNS immune functions and peripheral inflammatory signals is at the core of Alzheimer's disease pathogenesis. From BBB disruption and microglial dysfunction to complement activation and immune system infiltration, neuroinflammation is a driver and amplifier of neurodegeneration. An understanding of the temporal and spatial evolution of this process will be essential for defining optimal intervention windows and targets. With continued progress toward the development of treatments, attention to immune modulation and biomarker-driven approaches may lead to more successful treatments for AD [30].

The neuropathological characteristics of AD include extracellular amyloid-$\beta$ (A$\beta$) plaques and intracellular NFTs, which are made of hyperphosphorylated tau. The generation of neurotoxic A$\beta$ peptides arises from the amyloidogenic processing of APP , mediated sequentially by $\beta$-secretase and $\gamma$-secretase [35]. In AD, microglia and astrocytes are central to regulating neuroinflammation. Microglia, derived from early immune cells, become activated in response to AD pathology, migrating to damaged areas to clear debris and protein aggregates like A$\beta$. While acute activation aids in A$\beta$ clearance, chronic activation leads to harmful inflammation, promoting neuronal damage, synaptic loss, and increased A$\beta$ production.

Neuroinflammation in AD arises from the persistent activation of microglia and astrocytes, which release pro-inflammatory cytokines (TNF-$\alpha$, IL-1$\beta$, IL-6), chemokines, and reactive

oxygen species (ROS). Initially, this inflammatory response serves a protective function by clearing A$\beta$ aggregates and cellular debris. However, chronic activation leads to a self-perpetuating cycle of damage, where excessive cytokine production exacerbates neuronal injury and promotes further A$\beta$ deposition. Studies indicate that A$\beta$ oligomers trigger microglial activation via Toll-like receptors (TLRs) and inflammasome pathways. Astrocytes, influenced by activated microglia, also contribute to AD progression. Reactive astrocytes cluster near plaques and damaged regions, driving inflammation, while atrophic astrocytes, seen early in the disease, may disrupt synaptic connections due to reduced structural support. Together, these glial cells play a essential role in AD-related neurodegeneration [36].

## 2.2 Cytokines and Immune Signaling in AD

In AD, there is uniform evidence of elevated peripheral inflammatory marker levels, such as high-sensitivity CRP, IL-6, soluble TNFR1, $\alpha$1-ACT, and IL-1$\beta$. In addition, the raised CSF concentrations of IL-10 and MCP-1 indicate the occurrence of active neuroinflammatory processes. Collectively, these changes represent an intricate interaction between systemic inflammation and central nervous system immune activation in the pathogenesis of AD. High concentrations of pro-inflammatory cytokines in blood and CS) indicate an important contribution towards AD progression [37]. Microglial activation has both protective and pathological roles. Activated microglia promotes clearance of A$\beta$ during the acute phase by enhanced phagocytic activity, reducing its deposition. Chronic microglial activation, in contrast, can trigger uncontrolled neuroinflammatory reactions and contribute to neuronal dysfunction, synaptic damage, elevated A$\beta$ generation, and net neurotoxicity [38].

## 2.3 Tumor Necrosis Factor-Alpha and Memory

The need for innovative approaches is highlighted by the fact that numerous multinational pharmaceutical companies and research institutes spend billions of

dollars on anti-A$\beta$ or anti-tau strategies that don't work, despite the recent approval of aducanumab by the US FDA for the treatment of AD. Given its central role in AD, neuroinflammation presents a promising avenue for therapeutic intervention. Traditional anti-inflammatory drugs, such as NSAIDs, have shown mixed results in clinical trials, likely due to their broad mechanisms and late-stage administration. Researchers are employing pharmacology or genetics to create ways for depleting microglia because of the theory that microglia activation accelerates the course of AD. It has been demonstrated that depleting microglia in AD mice models produces positive outcomes. It is commonly known that CSF1R is an essential microglia surface receptor. In various AD mouse models, CSF1R inhibitors can reduce neuroinflammation, neuritic plaque buildup, dendritic spine loss, and enhance cognition [39].

## 2.4 Interleukin-1 Beta and Memory

One important pro-inflammatory cytokine of the IL-1 family, IL-1$\beta$, is extensively involved in the pathophysiology of AD. It is mostly produced by activated microglia in reaction to pathogenic stimuli such the buildup of A$\beta$. A primary cause of persistent neuroinflammation, which damages neurons and quickens the course of disease, is IL-1$\beta$. It is predominantly produced by activated microglia in response to pathological stimuli such as A$\beta$ accumulation.

IL-1$\beta$ is a major driver of chronic neuroinflammation, which contributes to neuronal damage and accelerates disease progression. Studies have shown that inhibition of the IL-1R in AD mouse models can significantly reduce tau hyperphosphorylation, a critical process involved in NFTs formation, and also improve cognitive function while modestly influencing A$\beta$ levels. Interestingly, IL-1$\beta$ has demonstrated paradoxical effects on amyloid pathology.

In certain experimental settings, overexpression of IL-1$\beta$ led to a marked reduction in A$\beta$ plaque burden, possibly due to enhanced microglial activation and A$\beta$ clearance, whereas in other contexts, it has been associated with increased A$\beta$ production through upregulation of $\beta$-secretase activity [14]. Additionally, IL-1$\beta$ impairs synaptic plasticity

by disrupting long-term potentiation (LTP), a key mechanism underlying learning and memory, thereby contributing to cognitive decline in AD.

Despite its detrimental inflammatory effects, the potential of IL-1$\beta$ to promote A$\beta$ clearance under specific conditions makes it a complex but compelling therapeutic target. Thus, while IL-1$\beta$ plays a largely harmful role in AD by sustaining neuroinflammation and promoting tau pathology, carefully modulating its signaling pathways may offer therapeutic benefits in altering disease progression [40].

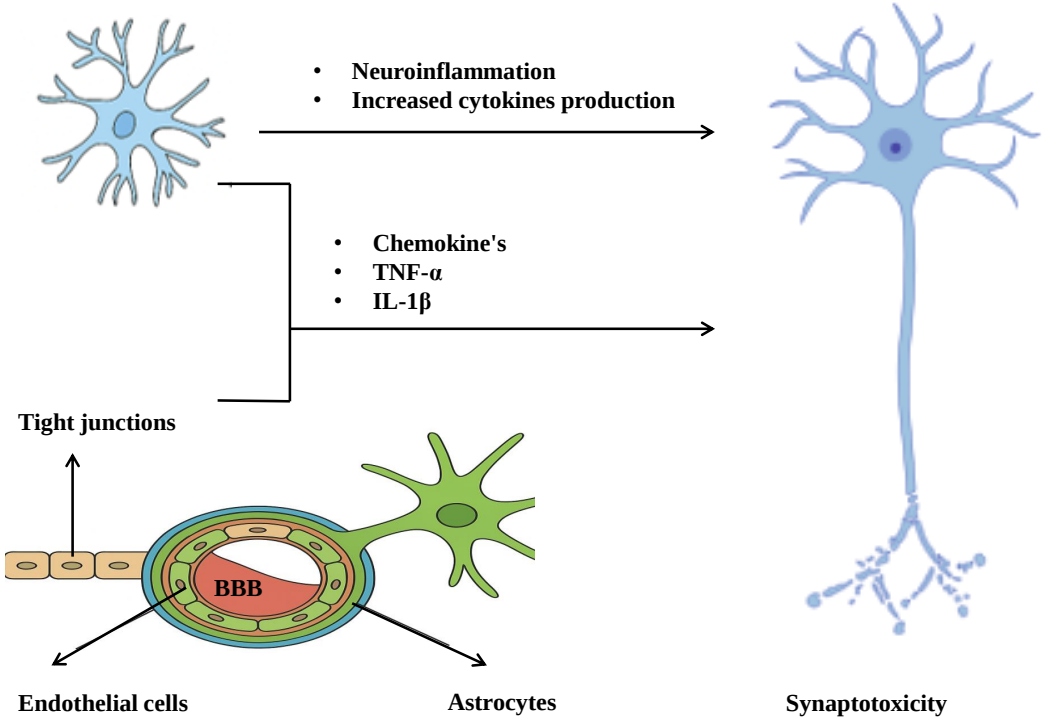


FIGURE 2.1: Mechanism of neuroinflammation in Alzheimer's disease (AD).

The above figure describes the activation of microglia and astrocytes, leading to increased production of pro-inflammatory cytokines including IL-1$\beta$, TNF$\alpha$, and chemokines.

These mediators disrupt the BBB, alter blood flow, and promote synaptotoxicity in neurons. The interaction among glial cells, endothelial cells, and neurons contributes to disease progression and neurodegeneration (Figure adopted by Onyango et.al 2021).

## 2.5 Nuclear Factor Kappa B and Memory

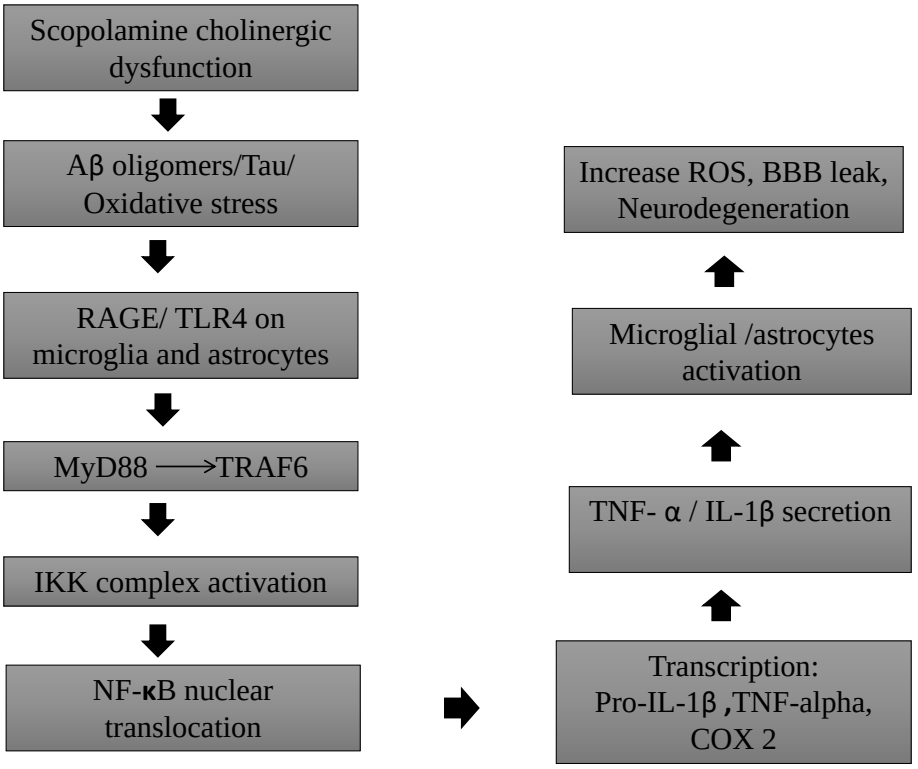


FIGURE 2.2: Schematic representation of NF-$\kappa$B–mediated neuroinflammation in a scopolamine-induced Alzheimer's disease model.

Scopolamine-induced cholinergic dysfunction, along with amyloid-$\beta$ (A$\beta$) accumulation, tau hyperphosphorylation, oxidative stress, and danger-associated molecular patterns (DAMPs), activates pattern recognition receptors such as RAGE and TLR4 on microglia and astrocytes. This triggers the MyD88–TRAF6–IKK signaling cascade, resulting in phosphorylation and proteasomal degradation of I$\kappa$B$\alpha$, thereby permitting NF-$\kappa$B (p65/p50) nuclear translocation. Activated NF-$\kappa$B induces transcription of pro-inflammatory mediators, including pro–IL-1$\beta$, TNF-$\alpha$, COX-2, and iNOS. In parallel, a secondary stimulus (ROS, $K^+$ efflux, lysosomal stress) promotes NLRP3 inflammasome assembly, leading to caspase-1 activation and cleavage of pro–IL-1$\beta$ into its mature, secreted form. The release of TNF-$\alpha$ and IL-1$\beta$ further amplifies microglial and astrocytic activation, exacerbates oxidative and nitrosative stress, compromises blood–brain barrier integrity, and accelerates synaptic dysfunction and neuronal loss.

## 2.6 Neuroinflammation Targeting Therapeutic Strategies for AD

This necessity is underscored by the reality that many multinational pharmaceutical firms and research centers invest billions of dollars annually on anti-A$\beta$ or anti-tau approaches that fail, even though the US FDA approved aducanumab for the treatment of AD recently. As a central mechanism of AD, neuroinflammation offers an attractive target for therapeutic intervention. Conventional anti-inflammatory medications, including NSAIDs, have been reported with inconclusive results in clinical trials, probably owing to their wide-ranging mechanisms and late-stage administration. Pharmacology or genetics are being used by researchers to design methods for depleting microglia owing to the hypothesis that microglia activation quickens the progression of AD. It has been proven that depleting microglia in models of AD results in favorable outcomes. It is widely recognized that CSF1R is a critical microglia surface receptor. In several models of AD, inhibitors of CSF1R can decrease neuroinflammation, neuritic plaque deposition, dendritic spine loss, and improve cognition [41].

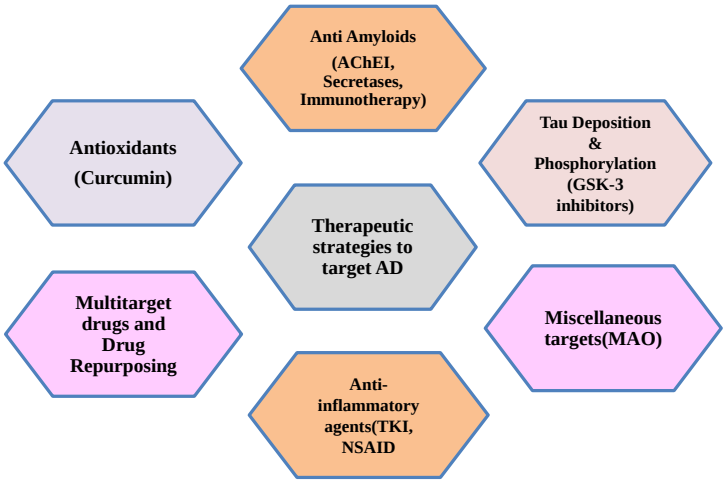


FIGURE 2.3: Therapeutic strategies of Alzheimer's disease (AD).

The above figure illustrates the multifactorial pathogenesis of AD and the corresponding diversity in therapeutic approaches under investigation. Central to these strategies are interventions targeting A$\beta$ pathology, including AChEIs, secretase

inhibitors, and immunotherapeutic agents, all aimed at reducing A$\beta$ accumulation and plaque formation in the brain. Concurrently, therapies directed against tau pathology, such as glycogen synthase kinase-3 (GSK-3) inhibitors, seek to prevent tau hyperphosphorylation and the development of neurofibrillary tangles. To address oxidative stress, a key driver of neuronal damage, antioxidants like curcumin are being explored for their neuroprotective potential. Likewise, the role of chronic neuroinflammation in AD progression has prompted investigations into anti-inflammatory agents, including tyrosine kinase inhibitors (TKIs) and non-steroidal anti-inflammatory drugs (NSAIDs). Another promising avenue involves the repurposing of existing drugs and the development of multitarget-directed ligands capable of modulating multiple disease pathways simultaneously. The current study aligns with this therapeutic framework by focusing on MBT derivatives, which exhibit both anti-inflammatory and antioxidant properties. These compounds are being evaluated for their ability to modulate neuroinflammatory pathways and oxidative damage, positioning them as potential multitarget therapeutic agents for the effective treatment of AD (Figure adopted by Teeba et.al 2021).

# Chapter 3

# Material and Methods

## 3.1 Animals

For the current studies, laboratory animals were handled and cared for according to the Guidelines published by the U.S based Association for Assessment and Accreditation of Laboratory Animal Care International (AAALAC). Male Balb/C mice of weight 25–30g were divided randomly into five groups (n=6) namely scopolamine group, treatment groups, donepezil-treated positive group, and saline control group. Mice employed in the present research were developed in the animal house of the Capital University of Science and Technology (CUST), Islamabad. Animals were kept in groups of six in a cage under controlled environmental conditions with a 12-hour light/dark cycle (lighting from 08:00 to 20:00), with free access to chow and water. All experimental procedures using animals were examined and cleared by the CUST Ethics Committee (Approval No. REC/FOP/F2024/03in compliance with institutional and international guidelines for the care and use of laboratory animals.

FIGURE 3.1: BALB/C mice utilized in study.

Laboratory animals were housed under standard laboratory conditions. These genetically consistent animals were used to ensure humane care and reliable experimental outcomes (photography taken at Faculty of Pharmacy, Capital University of Science and Technology, Islamabad).

## 3.2 Food Composition

Mice used in research were typically fed a balanced pellet diet designed to meet their nutritional needs. These ingredients were often included fish, flour, bran and powdered milk. Consistent and standardized diets ensured mice health and reliable experimental results.

TABLE 3.1: Composition of animal's food

| **Food item** | **5.0 Kg** | **10.0 Kg** | **20.0 Kg** | **40.0 Kg** |
|---|---|---|---|---|
| Wheat Flour | 3.25 Kg | 6.5 Kg | 13 Kg | 26 Kg |
| Chokar | 750 g | 1. 5 Kg | 3.0 Kg | 6.0 Kg |
| Fish | 750 g | 1. 5 Kg | 3.0 Kg | 6.0 Kg |
| Dry Skimmed Milk | 200 g | 400 g | 800 g | 1600 g |
| Vitamins/Minerals* | 75 g | 150 g | 300 g | 600 g |

## 3.3 Mice Handling

All experimental procedures involving mice were conducted in strict accordance with internationally accepted ethical standards for the care and use of laboratory animals, and were approved by the Ethics Committee of the Capital University of Science and Technology (CUST), Islamabad. Mice were acclimatized for seven days prior to the start of study for effective and reliable results. Before commencement of experimental procedures, all mice were allowed to acclimatize to the animal facility conditions for seven days. During this period, animals were monitored daily for signs of stress, illness, or abnormal behavior, and handled gently to minimize anxiety and habituate them to human contact [17]. Mice were identified by cage labeling also non-invasive marking techniques such as tail marking was done. Animals were randomly assigned into experimental and control groups using a simple randomization method to reduce bias. Gloves were worn and aseptic techniques were followed before starting handling Mice were gently but securely restrained by grasping them at the base of the tail and placing them on the wire cage lid. Using the opposite hand, the thumb and forefinger were positioned on the lower back while maintaining control of the tail. To ensure a firm yet humane grip, the loose skin at the nape of the neck was gently pinched and lifted, while the tail was guided toward the wrist and secured using the little finger. This method allowed for stable handling, minimizing stress while ensuring adequate ventilation and preventing escape.

FIGURE 3.2: Handling of laboratory mice during experimental procedures.

Throughout the experimental period, animals were monitored daily for clinical signs of discomfort, distress, or illness. Key parameters such as body weight, food and water intake, grooming behavior, and general activity were recorded. Any animal exhibiting signs of severe distress or poor health was humanely euthanized by cervical dislocation in accordance with institutional guidelines. The above figure shows that careful handling of a laboratory mouse using sterile latex gloves. Mice were acclimatized to the new environment for a period of seven days before starting of experiment. This acclimatization time helps the animals cope with housing conditions, minimizing stress and stabilizing physiological parameters, which is important for gaining accurate experimental results. After acclimatization, mice need to be handled gently and regularly using correct techniques like cupping with gloved hands. This approach minimizes fear and stress reactions, enhancing the animal's adaptation to human contact. Routine and humane handling maintains animal welfare and improves the quality and reproducibility of behavioral and drug research results (photography taken at Faculty of Pharmacy, Capital University of Science and Technology, Islamabad).

## 3.4 Mice Bedding

Mice were housed on bedding materials that provide comfort, absorb moisture, and reduce odor. Common bedding types include wood shavings (such as aspen) was used. Animal bedding was made with consideration of its potential impact on animal health, behavior, and the reliability of experimental outcomes. Bedding was changed on daily basis to provide them non-toxic, dust and stress-free environment for the mice.

FIGURE 3.3: Standard housing conditions for laboratory mice.

Mice used in the laboratory were housed in cages lined with corn cob bedding, a widely preferred substrate in experimental research due to its excellent moisture absorption, effective odor control, and ability to provide a clean, comfortable environment essential for maintaining animal health and well-being. Bedding was replaced daily to ensure hygiene, minimize ammonia buildup, and prevent microbial contamination. The cages, made of high-quality clear polycarbonate, were autoclavable, durable, and allowed unobstructed visual monitoring of the animals without causing disturbance. This setup supported natural exploratory and nesting behaviors, reduced stress levels, and contributed to the consistency and reliability of physiological and behavioral outcomes. Proper bedding and routine cage maintenance also helped prevent skin lesions, minimized dust-related respiratory distress, and promoted a stable, healthy research environment. (photography taken at Faculty of Pharmacy, Capital University of Science and Technology, Islamabad).

## 3.5 Animal Gender

The distance between the anal and genital orifices is used as a measure to differentiate between male and female, mouse and rat. This distance is greater in case of male while female has small distance between anal and genital orifices compared to male.

## 3.6 Randomization

To ensure unbiased allocation and remove data skew within test groups, randomization of animals was done before the study began. For easy identification throughout the course of experimental procedures, animals were marked on the tail with non-toxic, permanent ink. The marking process entailed the application of circular bands in different sizes and quantities with minimal spacing between them to ensure that the patterns remained clear. Particularly, Animal #1 was tagged with one small circular band around the tail, whereas Animal #2 was tagged with two small circular bands spaced evenly apart. Animal #3 and Animal #4 had

three and four small circular bands, respectively. Animal #5 was differentiated by one thick circular band. Finally, Animal #6 carried one thick circular band followed by one small one, with a small gap in between. This identification method allowed for regular monitoring and precise data collection on every animal during the study.

## 3.7 Euthanizing Methods

### 3.7.1 Dislocation

In 1972, the AAALAC Panel on Euthanasia approved cervical dislocation as a means of euthanizing mice. The AAALAC mandates that the procedure must render an animal unconscious within 15 seconds with minimal pain or distress, restricting its use to small rodents (<200g) handled by trained personnel. Since then, various methods have been employed to administer this treatment, each with its own set of methods to ensure a rapid and humane death. The hemostat-assisted cervical dislocation method consists of the operator yanking the tail of the mouse backward acutely in order to dislocate the cervical spine, while a large hemostat is inserted directly under the base of the skull. The manual dislocation of the cervical spine is done according to a similar principle but without the use of instruments; pressure is applied at the skull base by the thumb and forefinger of the operator, while the operator applies a sharp pull on the tail to obtain dislocation. In anterograde cervical dislocation, the tail is held firm with one hand while the other hand presses the top cervical spine downward and forward, sometimes with a twist, to dislocate the skull from the vertebrae without injuring the skin. A second variation, thoracic dislocation, has the thorax grasped at the caudal end of the ribcage by fore finger and thumb to fix the chest and then given a sudden pull on the tail to drive the thoracic vertebrae apart. Physiologically, dislocation severs brainstem-spinal connections, instantly deactivating the reticular activating system (responsible for consciousness) and preventing pain perception within 0.3 seconds. Death follows from diaphragmatic paralysis causing respiratory arrest and loss of

vasomotor tone leading to circulatory collapse. A secondary death confirmation method bilateral pneumothorax is mandatory post-procedure. Validation studies confirm isoelectric EEG readings within 0.5–2 seconds, absence of pain-associated behaviors (vocalization, limbic activation), and sustained AAALAC guidelines. All of these techniques are intended to cause fast unconsciousness and death with minimal pain and distress in accordance with ethical animal care [42].

FIGURE 3.4: Cervical dislocation technique in laboratory mice.

It ensures humane euthanasia of laboratory mice through cervical dislocation using a wooden spatula. The mouse is restrained gently, and the wooden spatula is applied firmly on top of the base of the skull while a rapid pulling action is made upon the tail, with separation of the cervical vertebrae being achieved. This technique induces instant loss of consciousness and death and allows a quick and least distressful procedure (photography taken at Faculty of Pharmacy, Capital University of Science and Technology, Islamabad).

### 3.7.2 Concussion

A concussion is a physical technique employed to cause euthanasia in small laboratory animals by the application of a forceful, directed impact against the skull. The trauma applied should be intense enough to result in the instant hemorrhage within the brain and inhibit the activity of the CNS with an instantaneous loss of consciousness. The mechanism of this method is the extremely rapid acceleration and deceleration of the head, which drives the brain into impact with the rigid inner surfaces of the skull. This sudden movement creates a severe change in intracranial pressure and induces structural damage to delicate neural tissues and vasculature, leading to disruption of vital neurological function. The force of the impact is meant to overwhelm the brain's ability to sustain consciousness, leading to a temporary state of being stunned or, in extreme situations, instant death. Physiologically, the concussion interferes with normal neural function by producing a mechanical disruption of the cerebral cortex and brainstem regions which regulate consciousness, breathing, and heart function. The acute trauma can produce damage to blood vessels with tearing of their walls, increased water within brain tissue (edema), and disruption of electrical transmission in critical brain areas. The combination of these occurrences effectively knocks out the animal's sensory input and motor output in a matter of milliseconds. Even with what appears to be simple application, this technique requires great technical accuracy and operator skill. The person conducting the procedure will need to have detailed knowledge of the anatomy of the animal, and especially where the brain is located and best striking point on the skull. The force needs to be sufficient to produce irreversible trauma but not so extreme that it will damage the carcass unnecessarily in the event that tissue preservation is necessitated by subsequent analysis. Misapplication, whether by insufficient force or by bad aiming carries a significant threat of failing to stun. A poorly stunned animal can stay awake or become awake again and experience increased pain, fright, and distress, all which are serious violations of animal welfare procedures.

Most importantly, concussion alone is not considered a humane or complete euthanasia technique by the leading regulatory institutions and ethical standards for

laboratory animal use, such as those of the AAALAC guidelines and other global authorities. It is technically defined as a stunning or rendering-insensible technique since its impacts can be reversible and short-term. Hence, the humane termination of life can only be assured by always having concussion immediately succeeded by a secondary, irreversible method such as cervical dislocation, exsanguination, or decapitation. This double procedure ensures that the animal cannot recover consciousness and that death is instantaneous. In scientific and veterinary contexts, concussion is typically only allowed where alternative approaches (chemical euthanasia) will compromise experiment results, for example, in pharmacokinetic or biochemical assays. Even in such cases, its application has to be ethically justified under strict ethical scrutiny, and the staff needs to be adequately trained and qualified to use this method with precision and consistency. Finally, although concussion is a quick and efficient way of making animals insensible, its use must be cautiously weighed against ethical, anatomical, and technical considerations. It must be contained within a larger euthanasia regime that respects the humane treatment of animals and makes use of internationally accepted welfare standards [42].

## 3.8 Chemicals and Drugs

Table 3.2: Structural Information of Selected Ligands

| Sr. No. | Chemical/Substance | Source |
|---|---|---|
| 1 | Scopolamine hydrobromide | Macklin (macklin.cn) |
| 2 | Donepezil tablet | Global Pharmaceutical Pvt. Ltd |
| 3 | Mercaptobenzothiazole (derivative) (Cyclohexylactamide) | Synthesized in lab / precursor from Sigma-Aldrich |
| 4 | Dimethyl sulfoxide (DMSO) | Sigma-Aldrich |
| 5 | Chloroacetyl chloride | Sigma-Aldrich |
| 6 | Dichloromethane | Sigma-Aldrich |
| 7 | Triethylamine | Sigma-Aldrich |
| 8 | Benzylamine | Sigma-Aldrich |
| 9 | Acetonitrile | Sigma-Aldrich |
| 10 | Potassium carbonate | Sigma-Aldrich |

Continued on next page

| Sr. No. | Chemical/Substance | Source |
|---|---|---|
| 11 | Potassium iodide | Sigma-Aldrich |
| 12 | Sodium sulphate anhydrous | Sigma-Aldrich |

Concluded

### 3.8.1 Mercaptobenzothiazole Derivative Source

| Code | Structure | Name | Color | Molecular Weight | Log Po/w |
|---|---|---|---|---|---|
| CMBT- 1 | 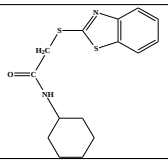 | 2-(Benzo[d]thiazol-2-ylthio)-n-cyclohexylacetamide | Shiny Brown | 306.45g/mol | 3.57 |

### 3.8.2 Scheme of Synthesis

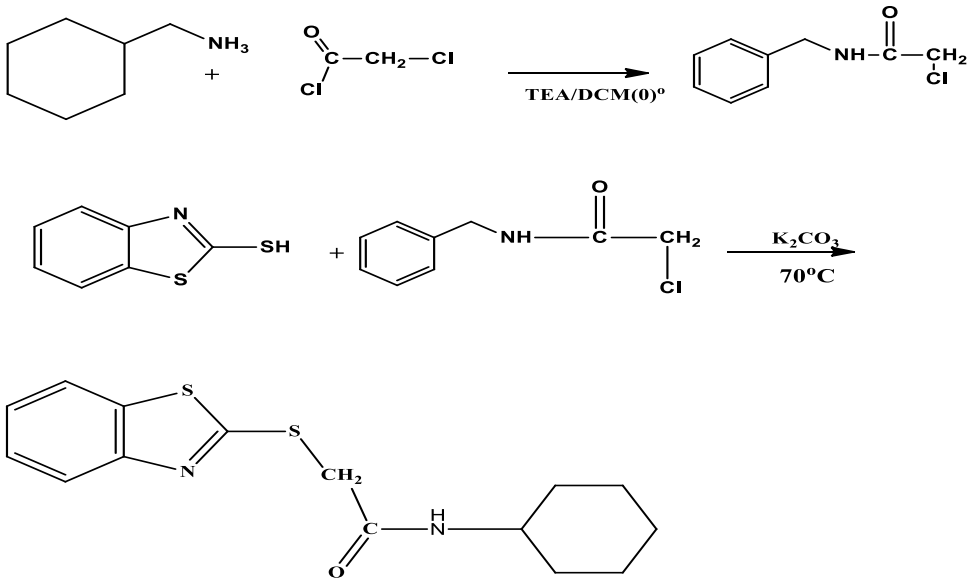


FIGURE 3.5: Synthesis of Benzo[d]thiazol-2-ylthio)-n-cyclohexylacetamide

We initially synthesized amides by reacting Cyclohexylamine with chloroacetyl chloride in the presence of triethylamine as a base and solvent used was dichloromethane, temperature should be maintained at zero degree. This reaction will take 4-5 hours to complete. The progress of reaction is monitored by doing TLC in 1:1 (Petroleum ether and ethyl acetate). After doing work up pure amides will be obtained which are further dried and used in next step for further reaction with 2 - mercaptobenzothiazole. This reaction will take place in acetonitrile solvent, temperature should

be maintained at 70-degree, base used was potassium carbonate and reaction take place in 3-4 days. After monitoring the progress of reaction by TLC in in 1:1 (Petroleum ether and ethyl acetate) we extract the mixture with ethyl acetate and isolate pure product.

## 3.9 Acclimatization

Mice were acclimatized to the laboratory environment for a period of seven days before the initiation of the experimental procedures. This acclimatization period allowed the animals to adjust to their new surroundings, minimizing stress and ensuring physiological and behavioral stability, which is essential for obtaining reliable and reproducible experimental results.

### 3.9.1 Grouping of Animals

Experimental animals were randomly assigned into five groups (n = 6 per group) based on their body weights to ensure uniform distribution. The treatment groups were organized as follows:

Group I (control group): Vehicle only.

Group II (negative control): Scopolamine at a dose of 1 mg/Kg to induce cognitive impairment.

Group III (positive control): Scopolamine (1 mg/Kg) + donepezil at a dose of 5 mg/Kg.

Group IV (test group I): Scopolamine (1 mg/Kg) + MBT at a dose of 5 mg/Kg.

Group V (test group II): Scopolamine (1 mg/Kg+ MBT at a dose of 10 mg/Kg.

### 3.9.2 Drug Administration

Before drug administration, each mouse was individually weighed to ensure accurate dose calculations for scopolamine, the MBT (cyclohexylactamide), and donepezil. Fresh solutions of all drugs were prepared regularly to maintain stability and efficacy.

The mice were randomly divided into five groups as follows:

**Group 1 (control):** Received an equivalent volume of vehicle (i.p.) and served as the control group.

**Group 2 (scopolamine-only):** Scopolamine at a dose of 1 mg/Kg (i.p.) once daily for seven consecutive days to induce Alzheimer's-like cognitive impairment.

**Group 3 (MBT low dose):** MBT at a dose of 5 mg/Kg (i.p.), 30 minutes before scopolamine administration.

**Group 4 (MBT high dose):** MBT at a dose of 10 mg/Kg (i.p.), 30 minutes before scopolamine administration.

**Group 5 (donepezil):** Donepezil at a dose of 5 mg/Kg (p.o.), 30 minutes before scopolamine administration.

All drug administrations were carried out under sterile conditions and performed at the same time each day to minimize circadian variability. Intraperitoneal injections were used for rapid systemic absorption, except for donepezil, which was administered orally to mimic clinical use.

FIGURE 3.6: Intraperitoneal (i.p.) drug administration in mice.

The above figure demonstrates i.p. administration in a laboratory mouse, with injection being given in the lower right quadrant of the abdomen. This location is chosen to stay away from critical organs like the bladder, cecum, and intestines to minimize the chance of damage. A sterile insulin syringe (usually 1 mL with a 26–30-gauge needle) is utilized for accurate and least disruptive delivery of the test substance. The mouse is gently held in place, and the needle is placed at a shallow angle (15–30°) into the right lower quadrant of the abdomen. The syringe is checked for blood or fluid absence before injection to ensure proper placement. This method is frequently used for drug delivery because of its fast systemic absorption, and should be carried out under strict aseptic to facilitate animal welfare and reliability of experimental results (photography taken at Faculty of Pharmacy, Capital University of Science and Technology, Islamabad).

### 3.9.3 Drug Solubility

As the test compound was poorly soluble in water, an initial attempt was made to dissolve it in normal saline with vortexing. However, due to limited solubility, a co-solvent approach was employed. Specifically, 40 $\mu$L of dimethyl sulfoxide (DMSO) was added to an eppendorf tube containing the compound, and the mixture was vortexed thoroughly to ensure complete dissolution. Following this, 950 $\mu$L of normal saline was added to the solution and vortexed again to obtain a final volume of 1 mL. This preparation ensured a homogenous and stable drug solution suitable for intraperitoneal administration.

### 3.9.4 Dose Preparation

For the preparation of a 5 mg/Kg drug solution (1 mL), 0.5 mg of the drug was initially dissolved in 40 $\mu$L of dimethyl sulfoxide (DMSO) in a sterile eppendorf tube. Subsequently, 950 $\mu$L of normal saline was added, and the solution was vortexed thoroughly to ensure complete dissolution. The drug was fully soluble in DMSO before dilution.

To prepare a 10 mg/Kg drug solution (1 mL), 1 mg of the drug was first dissolved in 40 $\mu$L of DMSO, followed by the addition of 950 $\mu$L of normal saline. The mixture was then vortexed to obtain a clear and homogeneous solution, confirming complete dissolution of the drug in DMSO before dilution. For scopolamine solution, 0.1 mg of scopolamine was accurately weighed and dissolved in 1 mL of distilled water. The solution was stirred properly to ensure complete dissolution before administration.

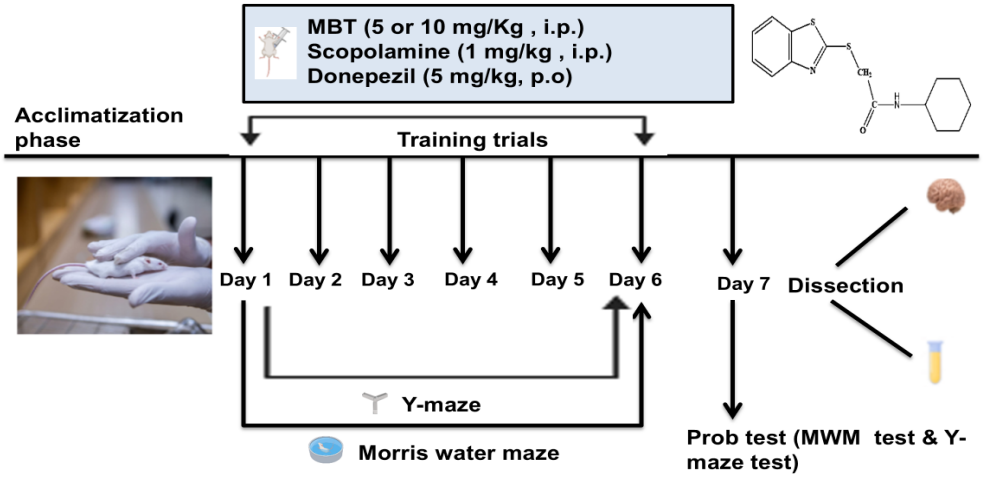


FIGURE 3.7: Experimental design illustrating the scheme and study plan for scopolamine-induced Alzheimer's disease (AD).

The above diagram shows experimental design for evaluating the effects of MBT at doses of 5 and 10 mg/Kg (i.p.) in a scopolamine-induced mouse model of AD. After acclimatization, animals underwent behavioral testing using the MWM and Y-maze from Day 2 to Day 6, followed by a probe test and brain dissection on Day 7 for biochemical and histological analysis.

## 3.10 Y-Maze Test

The Y-maze equipment was made up of three white arms at 120° angles to one another, with the size of each arm as 20 cm lengthwise, 6 cm widthwise, and 10 cm height wise. Mice were acclimatized to the Y-maze condition before the treatment started. Mice were set at the beginning of one allocated arm (initial position) at the beginning of every trial. Arms A, B, and C were marked, and the order and frequency of arm entries were captured on a video camera. An entry was only tallied when the entire body of the mouse, including its tail, had completely entered the arm. Spontaneous alteration behavior was characterized as consecutive entries into all three arms without repeated entry to the same arm (ABC, BCA, or CAB sequences). Percentage of spontaneous alternation was determined using the formula: % Alternation = [Number of actual alternations / (Total arm entries - 2)] × 100. In the current study, scopolamine injection significantly decreased the percentage of spontaneous alternation, reflecting compromised spatial working memory. Still, donepezil treatment alongside MBT at doses of 5 mg/Kg and 10 mg/Kg caused a significant increase in spontaneous alternation, indicating improvement in cognitive function [43].

FIGURE 3.8: Y-maze apparatus for spatial learning memory assessment in mice.

The Y-maze apparatus was constructed from stainless steel, used to evaluate spontaneous alternation behavior in rodents, which reflects spatial working memory. Each of the three identical arms extends at 120° angles from a central point. The mouse is placed at the start arm and allowed to explore freely, and its choices are recorded to assess cognitive performance, in models of Alzheimer's disease

(photography taken at Faculty of Pharmacy, Capital University of Science and Technology, Islamabad).

## 3.11 Morris Water-Maze Test

The behavioral tests were done in a MWM placed inside a circular steel tank. The tank was made of stainless steel, which was highly durable, resistant to chemicals, and easy to clean between trials. The diameter of the tank was 135 cm, and the height was 42 cm. It was filled to a depth of about 40 cm with water. The temperature of the water was kept at $22 \pm 2$ °C, within the optimal range for rodent behavior testing to prevent hypothermia or stress. White powdered non-toxic milk was added to make the water opaque in order to block visibility of the escape platform and avoid proximal visual cues in the water that can be used by the mice.

The interior wall of the tank was split into four equal virtual quadrants via geometric markings on the walls surrounding the tank. Each quadrant was identified using distinctive extramaze visual cues like patterned symbols or color-coded flags mounted above the rim of the tank. These stimuli were maintained constant throughout the experiment to facilitate the mice to form spatial associations.A 10 cm diameter, 25 cm high circular escape platform, constructed from transparent acrylic material, was placed in one quadrant (labeled the target quadrant) and submerged 1 cm below water level, making it invisible to the mice.

Pre-training acclimatization was also done to reduce novelty-induced stress and habituate the animals with the test environment, and to this end, a two-day acclimatization period was implemented. During this period, the platform was removed, and each mouse was left to swim freely in the tank for a short period (30–60 seconds) per day. This exposure allowed animals to get used to water and the spatial cues of the area without any reward from the platform. At training trials was carried out for six consecutive days, with a single trial per mouse per day. At the start of every trial, the platform was positioned in the same place (target quadrant). Each mouse was released into the water from a different start quadrant, which was randomized every day to

avoid the learning of non-spatial search strategies. The mouse was given a maximum of 60 seconds to find the submerged platform using distal cues after being released. If successful, the mouse was allowed to be placed on the platform for 15 seconds as a reward and to support spatial learning. If the mouse did not find the platform.within the time limit, it was guided to the platform gently and left to stay on the platform for the same amount of time. This provided continuous exposure to learning in all subjects irrespective of starting performance. Trial escape latency (time it took to find the platform), path length, and swimming measure were tracked during each trial with an overhead video camera and processed with tracking software. On day seven, a probe trial was performed to assess spatial memory retention and consolidation. During this session, the escape platform was taken away from the tank. All the mice were placed in the water from the quadrant diametrically opposite to the target quadrant in order to eliminate bias due to earlier entry points. Mice were placed freely in the water for 60 seconds, during which their activities were observed. The main parameter recorded was time spent in the target quadrant where the platform was placed during training. A higher duration in the target quadrant indicates successful spatial learning and memory consolidation.In addition to time spent in each quadrant, number of platform crossings (swims over the exact location of the former platform), search strategy, and preference for the correct quadrant were also evaluated during the probe test. All experimental sessions were conducted under uniform lighting and noise-controlled conditions to minimize external interference [44].


FIGURE 3.9: MWM apparatus for assessment of spatial learning and memory in mice.

The MWM apparatus consists of a large circular tank filled with opaque water

to obscure a hidden platform submerged just below the surface. During the test, the mouse is released into the water from various starting points and must rely on distal visual cues to locate the platform. Repeated trials allow researchers to assess the animal's ability to learn and remember the location of the platform over time. Key parameters analyzed include escape latency, and time spent in the target quadrant during the probe trial. The test is sensitive to hippocampal-dependent memory impairments, making it a crucial tool in cognitive impairment assessment (photography taken at Faculty of Pharmacy, Capital University of Science and Technology, Islamabad).

## 3.12 Molecular Docking Studies

Molecular docking simulations were carried out using a combination of computational tools, including PyMOL (v3.0.4), AutoDock (v1.5.7), Discovery Studio (v2017), and ChemDraw. ChemDraw was employed to draw and visualize the chemical structures of ligands, while PyMOL (v3.0.4) was used for the three-dimensional visualization and structural inspection of protein-ligand complexes. Docking studies were primarily conducted using AutoDock Tools (v1.5.7), which facilitated the preparation of ligands and receptors and enabled flexible ligand docking simulations. Additionally, Discovery Studio (v2017) was utilized for post-docking analysis, including interaction profiling, binding energy visualization, and generation of 2D interaction diagrams. Donepezil hydrochloride was used as a reference standard in the docking studies. These computational analyses helped predict the binding affinity and possible molecular interactions of selected ligands with target proteins, thereby contributing to the understanding of their potential mechanisms of action.

## 3.13 Ligand Preparation

All of the chosen MBT derivatives as well as standard donepezil were loaded into Discovery Studio as mol files. After minimizing the energy of each ligand and

saving it in pdb format, they were all imported into the Autodock program, where they were charged and saved in pdbqt format.

### 3.13.1 Protein Preparation

The target protein structures were captured against various receptors IL-1$\beta$, TNF$\alpha$ and NF-$\kappa$B by using PDB ID: 8c3u, 7jra and 9bdw from PDB (Protein data bank) (http://www.rcsb.org). The structure of the proteins was built using the Discovery studio to clean protein and autodock tool is used to save protein in pdbqt format. Dog site scorer is used to find the active site and pymol is used to sequence the residue. Grid was built by identifying the specific residues involved in the active zone of the target proteins. Now proteins were ready for docking.

### 3.13.2 Ligand Docking

The 3D structures of the substituted compounds were generated using ChemBio-Draw. Molecular docking studies were conducted using AutoDock tool, targeting the protein structure with PDB ID: 8c3u. Discovery Studio Visualizer was employed to analyze the binding interactions and identify the most favorable binding conformations, based on lower binding free energy. The docking results were evaluated using a root mean square deviation (RMSD) threshold of 2.0 Å to ensure the reliability of the binding poses. The optimal docking conformation was selected based on its relatively low binding free energy. Key amino acid residues involved in ligand-protein interactions were further analyzed through both three-dimensional (3D) and two-dimensional (2D) visual representations.

### 3.13.3 Toxicity Studies

To evaluate the potential toxicological properties of the compound MBT (cyclohexylactamide), two *in silico* predictive tool **ToxTree** (version X.X) and **ProTox** were employed. These computational tools were used to assess various toxicity endpoints based on the chemical structure of the compound. ToxTree**,** an open-source

application developed by Idea consult Ltd., was used to determine the toxic hazard classification of MBT based on decision tree approaches. The software applies a series of structure-based rules and QSAR (Quantitative Structure–Activity Relationship) models to predict toxicological profiles, including: Cramer classification (to evaluate oral toxicity potential), Genotoxic carcinogenicity, Mutagenicity

The chemical structure of MBT was drawn using ChemSketch and exported in SMILES format. The SMILES string was then input into ToxTree, and toxicity predictions were recorded for further analysis and interpretation. ProTox-II, a web-based virtual laboratory for the prediction of rodent oral toxicity, toxicity endpoints, and toxicity pathways, was also utilized. This tool uses a combination of machine learning algorithms and structural similarity to known compounds to estimate toxicity parameters such as:, LD50 values, Toxicity class (according to GHS classification) and predicted organ toxicity (e.g., hepatotoxicity, cytotoxicity) The MBT compound structure was uploaded in SMILES format, and the software provided a comprehensive report outlining the predicted oral toxicity level and possible toxic effects on target organs and biological pathways. All analyses were performed under standardized settings as recommended by the respective platforms. The results obtained from both ToxTree and ProTox were used to compare and cross-validate the *in- silico* predictions, providing an initial toxicological profile of MBT (Cyclohexylactamide) for further experimental consideration.

## 3.14 Quantification of Hippocampal Protein Concentration via Bicinchoninic Acid

For determination of hippocampal tissue samples' total protein concentration before enzyme-linked immunosorbent assay (ELISA), the BCA assay was conducted with a commercial BCA Protein Assay Kit (Biosharp, Catalogue No: BL521A). Precise protein determination is an essential preparatory measure ahead of ELISA for the assurance of equal protein loading and comparative analysis among experimental groups. The hippocampus, a midbrain structure that has strong relations with

learning and memory, was first separated from every animal and homogenized right away in radioimmunoprecipitation assay buffer in a 1 mL for every 100 mg of tissue ratio. Homogenizing was done on ice to maintain protein integrity, and then centrifugation at 8,500 rpm for 30 minutes at room temperature was done. The supernatant thus obtained with solubilized proteins was carefully harvested and preserved at 20°C until analysis.

For the BCA assay, 10 $\mu$L of each hippocampal sample was added to the wells of a 96-well microplate. Serial dilutions of bovine serum albumin with concentrations of 0 $\mu$g/mL, 7.5 $\mu$g/mL, 10 $\mu$g/mL, 15 $\mu$g/mL, and 20 $\mu$g/mL, all in triplicate, were used to create the standard curve. The working BCA reagent was newly prepared by combining Reagent A and Reagent B in a 50:1 ratio as suggested by the manufacturer. The working reagent of 200 $\mu$L was added to every sample and standard well. The plate was then incubated at 37°C for 30 minutes to allow color development. Following this, absorbance was read at 562 nm in a Thermo Fisher Multiskan microplate reader. The absorbance values obtained for the standard curve showed a good linear correlation with protein concentration (e.g., 0.800 at 20 $\mu$g/mL, 0.588 at 15 $\mu$g/mL, 0.468 at 10 $\mu$g/mL, and 0.234 at 7.5 $\mu$g/mL), which proved the reliability of the assay for protein estimation. Protein concentrations were calculated using this standard curve for each sample in all experimental groups. In the control group, protein levels in the hippocampus were generally high and ranged from 10.12 to 17.75 $\mu$g/mL, demonstrating intact neuronal function and structure. In the scopolamine-treated group, there was a sharp decline in protein content, ranging from 7.24 to 10.30 $\mu$g/mL, denoting extensive neurodegenerative changes typical of the memory impairment that follows scopolamine treatment. Donepezil treatment in scopolamine-challenged mice resulted in a partial restoration of protein levels between 10.40 and 13.73 $\mu$g/mL, which indicated some neuroprotection. Intriguingly, animals treated with MBT (cyclohexylacetamide) at 5 mg/Kg had protein concentrations between 9.38 and 17.40 $\mu$g/mL, where some samples approached the control level. Still more dramatic, the MBT-treated group at 10 mg/Kg had protein consistently higher than the others, with a range of 13.91-17.47 $\mu$g/mL, comparable to that of the control group and higher than the donepezil group. These findings firmly support the hypothesis that MBT has a dose-dependent neuroprotective action in retaining hippocampal protein content, and warrant its potential therapeutic candidacy against scopolamine-induced

neuronal injury. The protein concentrations determined by the BCA assay were then applied for normalization of protein loading in ELISA assays to detect the inflammatory cytokines IL-1$\beta$ and TNF-$\alpha$ of the hippocampus [44].

FIGURE 3.10: Microplate reader thermo scientific multiskan FC.

The Microplate reader is used for measuring absorbance at 562 nm during the Bicinchoninic Acid (BCA) protein assay. A 96-well plate containing hippocampal tissue lysates and BSA standards was loaded into the reader to quantify total protein concentrations (photography taken at Faculty of Pharmacy, Capital University of Science and Technology, Islamabad).

## 3.15 Determination of Hippocampal IL-1$\beta$ and TNF-$\alpha$ Levels via Sandwich ELISA

To determine the neuroinflammatory state in model mice, quantitative IL-1$\beta$ and TNF-$\alpha$ levels were measured by the ELISA. These cytokines are key biomarkers of neuroinflammation, and their overexpression within the hippocampus has been centrally associated with neurodegenerative mechanisms, including those seen in models of Alzheimer's disease. A commercially available sandwich ELISA kit was utilized for this, Pars Biochem ELISA Kit for mouse IL-1$\beta$ (Catalogue No: PRS-20295Mo, Lot No: 202312, sensitivity <2 pg/mL, assay range 15.6–1000 pg/mL) and Pars

Biochem ELISA Kit for mouse TNF-$\alpha$ (Catalogue No: PRS-20505Mo, Lot No: 202312, sensitivity <3 pg/mL, assay range 31.2–2000 pg/mL) and all the steps were carried out in strict compliance with the manufacturer's guidelines. Following behavioral examinations, mice were sacrificed and the brains quickly dissected on ice. The hippocampus was dissected under sterile conditions with caution and homogenized in phosphate-buffered saline (PBS) with the inclusion of protease inhibitors to preserve native protein structure. Homogenates were centrifuged at 12,000 rpm for 15 minutes at 4°C, and resultant supernatants were collected for analysis of cytokines. Protein levels were quantified by the Bradford assay for maintaining consistency of sample input for ELISA. The ELISA was carried out in 96-well microplate format, in which wells were pre-coated with monoclonal antibodies against mouse IL-1$\beta$ or TNF-$\alpha$. Standards were reconstituted and serially diluted on the plate to generate a standard curve from the maximum concentration available. Sample dilutions were done at a ratio of 1:5 by mixing 10 $\mu$L of hippocampal supernatant with 40 $\mu$L of sample diluent. 50 $\mu$L of each standard or diluted sample was then pipetted into the appropriate wells. Accuracy was ensured by running samples and standards in duplicate. Blank wells containing just diluent were also included to get background absorbance. The plates were then sealed and incubated at 37°C for 30 minutes to allow the cytokines to reversibly and specifically bind to immobilized capture antibodies. Wells were washed five times with a wash buffer (20–30-fold diluted concentrate with distilled water) after incubation, to eliminate unbound material. Subsequently, 50 $\mu$L of horseradish peroxidase (HRP)-conjugated detection antibody was added to all the wells except blanks and incubated at 37°C for 30 minutes. Following a second series of wash steps to remove excess detection antibody, 50 $\mu$L of Chromogen Solution A and 50 $\mu$L of Chromogen Solution B were added to all the wells. The plate was incubated in darkness at 37°C for 15 minutes to achieve color development, during which the enzymatic reaction catalyzed by HRP generated a blue chromophore. The enzyme reaction was arrested by adding 50 $\mu$L of Stop Solution, whose color changed from blue to yellow. The absorbance was measured at 450 nm using a microplate reader 15 minutes after reaction arrest to ensure accuracy of the data. OD measurements for all samples were matched against the standard curve to determine cytokine levels. The results were expressed as picograms per milliliter (pg/mL) and statistically analyzed to contrast treatment groups. ELISA

technique provided reproducible and trustworthy quantitation of IL-1$\beta$ and TNF-$\alpha$ material present in hippocampal tissue, which provided valuable information on the extent of neuroinflammatory response and therapeutic action of the drug administered [45].


FIGURE 3.11: Primary coated antibody 96 well plates for ELISA.

The above figure shows quantitative analysis of pro-inflammatory cytokines IL-1$\beta$ and TNF-$\alpha$ as measured by ELISA. Each well contains samples or standards processed to detect and quantify cytokine levels indicative of inflammatory response (photography taken at Faculty of Pharmacy, Capital University of Science and Technology,) Islamabad.

## 3.16 Histopathological Evaluation of Hippocampal Tissue using Hematoxylin and Eosin

For evaluating tissue architecture and pathological changes, histological staining was carried out by the H&E method, a well-established technique for overall tissue morphology. Formalin-fixed tissue samples were first processed by routine histological methods. Tissues were fixed in 10% neutral-buffered formalin for 24-48 hours at room temperature to retain morphological integrity. After fixation, the samples were dehydrated in a graded series of ethanol (70%, 80%, 95%, and 100%), cleared in xylene, and then embedded

in paraffin wax with the aid of an automated tissue processor. Paraffin-embedded tissue blocks were cut into 4-5 $\mu$m thick sections on a rotary microtome. The sections were mounted on clean glass microscope slides and dried overnight at 37°C, or for 1 hour at 60°C to improve adherence before staining. For H&E staining, the slides were deparaffinized initially by soaking in xylene (two changes, 5 minutes each) to dissolve paraffin. This was followed by rehydration in a descending series of alcohol (100%, 95%, and 70% ethanol) and rinsed briefly in distilled water. Sections were then stained with Harris's hematoxylin solution for 5–7 minutes to stain cell nuclei, and then rinsed in running tap water to drain off excess stain. Differentiation was done, if needed, with 1% acid alcohol (1% HCl in 70% ethanol) for a few seconds to eliminate non-specific nuclear staining, and nuclear bluing was done by submerging the slides in 0.2% ammonia water or alkaline tap water for 1 minute. Then cytoplasmic and extracellular material was counterstained with 1% eosin Y solution for 30 seconds to 1 minute. Following staining with eosin, the slides were quickly washed in distilled water to avoid over staining. The stained sections were dehydrated through an increasing series of concentrations of ethanol (70%, 95%, and 100%) and cleared in xylene (two changes, 3 minutes each). Coverslips were finally mounted in a xylene-based permanent mounting medium to fix the stained sections. The stained slides were permitted to air dry thoroughly and were viewed under a bright-field light microscope at different magnifications (10×, 40×) to assess cellular morphology, tissue architecture, and histopathological alterations. Representative photographs were taken for documentation and analysis [46].

## 3.17 Statistical Analysis

All experimental data obtained from behavioral, biochemical, and histological assays in this study were analyzed using GraphPad Prism version 8.0.2, a robust and widely accepted software for statistical evaluation and scientific data visualization in biomedical research. For evaluating inter-group differences, particularly among the control, scopolamine-treated, donepezil-treated, and MBT low-dose and high-dose groups, a one-way analysis of variance (ANOVA) was applied to biochemical (cytokine levels), histological, and static behavioral endpoints. In contrast, for

behavioral tasks involving repeated measures over time, such as escape latency in the Morris Water Maze or percentage spontaneous alternation in the Y-maze, a two-way ANOVA was performed with treatment and day (or time) as independent factors. Following a statistically significant main effect or interaction in either ANOVA model, Tukey's post hoc multiple-comparison test was conducted to determine specific differences between groups. Tukey's test was selected for its ability to control the family-wise error rate and to facilitate all possible pairwise comparisons.

For all comparisons, a P-value of less than 0.05 ($P < 0.05$) was considered statistically significant. Where applicable, exact P-values ($P = 0.032$) were reported for transparency. Results were annotated with increasing levels of statistical significance using standard notations: *$P < 0.05$, **$P < 0.01$, and **$P < 0.001$ to enhance interpretability.

All data are presented as mean ± standard error of the mean (SEM), reflecting group variability and allowing inference to the population level. GraphPad Prism was also utilized to generate bar graphs, time-course plots (escape latency across days) to represent the behavioral outcomes of MBT treatment in scopolamine-induced AD models.

To uphold data integrity and minimize bias, the entire data analysis process was conducted under blinded conditions, where the individual performing the analysis was unaware of the group allocations throughout data entry and interpretation.

# Chapter 4

# Results

## 4.1 Acute Toxicity

During the initial acute toxicity observation period, intraperitoneal (i.p.) administration of the test compound, mercaptobenzothiazole (MBT), at a dose of 100 mg/Kg body weight, was evaluated in adult mice to assess its safety profile before pharmacological testing. Following administration, animals were continuously monitored for the first 4 hours post-injection and subsequently observed twice daily for a period of 3 days for any signs of acute toxicity or adverse behavioral changes. Parameters assessed included locomotor activity, grooming behavior, food and water intake, posture, respiration, salivation, tremors, reflex and responsiveness. In addition, body weight measurements were recorded daily to detect any treatment-related systemic effects. Throughout the observation period, no mortality occurred, and animals exhibited no signs of distress, morbidity, or significant behavioral abnormalities. Importantly, there were no statistically significant changes in body weight, suggesting that MBT at this dose did not interfere with normal metabolic or physiological functions. The absence of acute toxicity symptoms at the 100 mg/Kg i.p. dose indicates that MBT was well-tolerated and non-lethal in the administered concentration, fulfilling the preliminary safety criteria for in vivo experimentation. This aligns with established toxicological frameworks, where substances showing no

lethality or severe clinical symptoms at test doses are considered safe for subchronic or chronic pharmacological evaluations

## 4.2 Behavioral Assessment

### 4.2.1 Effect of MBT Compound on Spatial Memory Deficit in MWM Test

In the MWM test, the group administered with scopolamine showed a significant ($P < 0.001$) increase in escape latency when compared to the control group (Figure 16). However, a notable decrease ($P < 0.001$) in escape latency was noted in the group that received MBT compound (5 mg/Kg, 10 mg/Kg). According to the probe trial, mice treated with scopolamine spent less time in the target quadrant than the vehicle control group, but mice treated with MBT compound (5, 10 mg/Kg) spent significantly more time ($P < 0.001$) in the target quadrant than the negative control group.

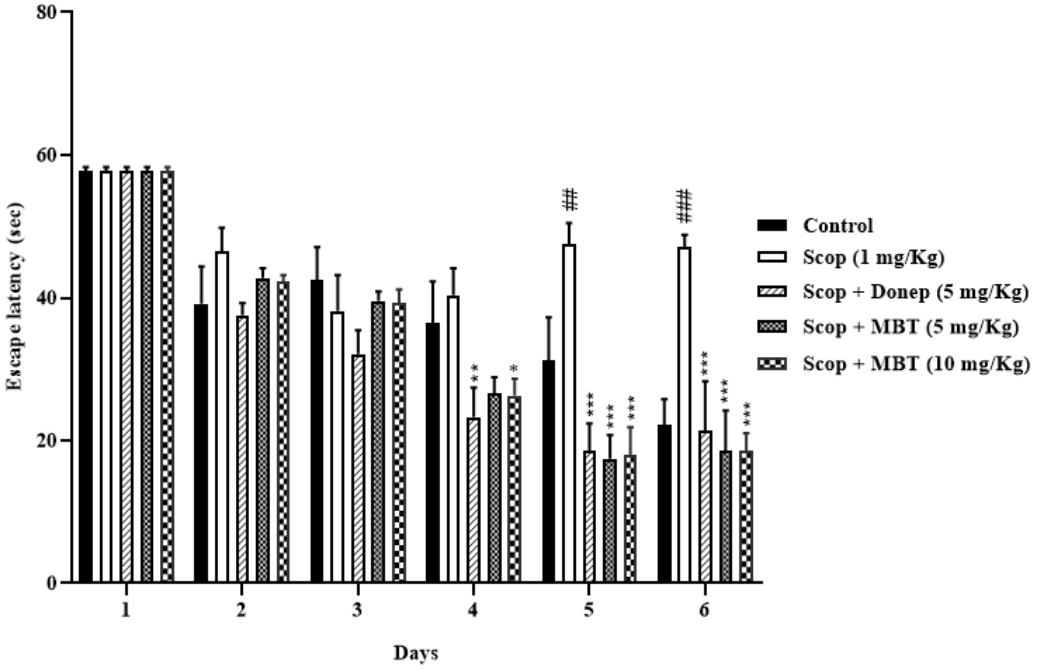


FIGURE 4.1: Effects of MBT compound on escape latency in MWM.

In this study, scopolamine (1 mg/Kg, i.p.) was administered once daily for 7 consecutive days to induce memory deficits. Treatments, including donepezil (5 mg/Kg) and MBT (5 or 10 mg/Kg), were given 30 minutes before scopolamine administration. Mice treated with scopolamine alone exhibited a significant increase in escape latency in the MWM test, indicating impaired spatial learning and memory. In contrast, pre-treatment with donepezil or MBT significantly attenuated scopolamine-induced cognitive deficits, as evidenced by reduced escape latency. Data are expressed as mean ± SEM (n = 6). Statistical significance was denoted as *P < 0.05, **P < 0.01, ***P < 0.001 vs. the scopolamine-treated group; #P < 0.05 and ###P < 0.001 vs. the control group.

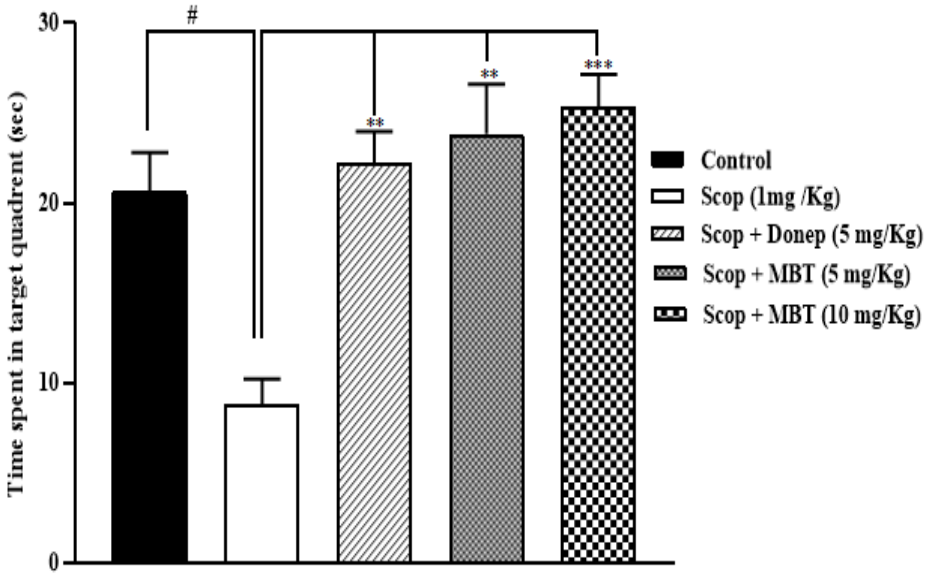


FIGURE 4.2: Effects of MBT compound on time spend in target quadrant in MWM.

Scopolamine (1 mg/Kg, i.p.) was administered daily for 7 days to induce memory impairment in the current study. The treatments were administered 30 minutes prior to scopolamine administration. On day 7 prob test was conducted, it was noted that mice treated with scopolamine show marked decrease in time spent in target quadrant in MWM test. However, donepezil (5 mg/Kg) and MBT (5 & 10 mg/Kg) significantly increase the time spent in target quadrant in scopolamine-induced MWM test. Data were presented as mean ± SD (n = 6). *P < 0.05, **P < 0.01 and ***P < 0.001 versus the scopolamine-treated group, #P < 0.05 and ###P < 0.001 represent significance between scopolamine and control group.

### 4.2.2 Effect of MBT Compound on Spatial Memory Deficit in Y-Maze Test

The Y-Maze test showed that the mice administered with scopolamine had a significantly lower percentage of spontaneous altered behavior ($P < 0.05$) than the mice in the control group (Figure 18). In contrast, MBT (5, 10 mg/Kg i.p.) 30 minutes before scopolamine administration markedly enhanced ($P < 0.001$) the spontaneous alteration behavior seen in y-maze test hence improving memory.

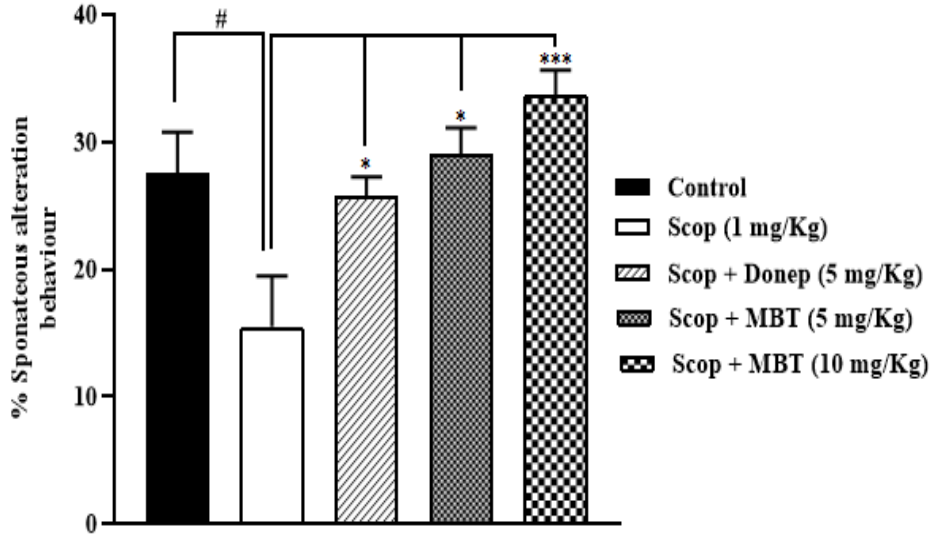


FIGURE 4.3: Effects of MBT compound on % spontaneous alteration in y-maze test.

Scopolamine (1 mg/Kg, i.p.) was administered daily for 7 days to induce memory impairment in the current study. The treatments were administered 30 minutes prior to scopolamine administration. The results indicate that mice treated with scopolamine show marked decrease in % spontaneous alteration behavior in Y-maze. However, donepezil (5 mg/Kg) and MBT (5 & 10 mg/Kg) significantly increase the % spontaneous alteration behavior. Data were presented as mean ± stocktickerSEM (n = 6). *$P < 0.05$, **$P < 0.01$ and ***$P < 0.001$ versus the scopolamine-treated group, $^{\#}P < 0.05$ represent significance between scopolamine and control group. Spontaneous alteration behavior in the scopolamine-treated mice in comparison to the control group mice. While, treatment with MBT (5 & 10 mg/Kg, i.p.) 30 min before scopolamine administration, significantly improved

the memory by remarkably increasing ($P < 0.001$) the spontaneous alternation behavior observed in Y-maze test.

## 4.3 Effects of MBT on Proinflammatory Cytokines Expression in Hippocampus of Mice Assessed by ELISA

### 4.3.1 Tumor Necrosis Factor

The quantitative estimation of tumor necrosis factor-alpha (TNF-$\alpha$) in hippocampal tissue was performed using enzyme-linked immunosorbent assay (ELISA), with standard curves generated from known concentrations ranging from 0 to 90 $\mu$g/ml. The standard absorbance values showed a strong linear trend, with 2.532 at 90 $\mu$g/ml, 1.721 at 60 $\mu$g/ml, 0.981 at 30 $\mu$g/ml, 0.7011 at 15 $\mu$g/ml, and 0.407 at 7.5 $\mu$g/ml, establishing assay sensitivity and reliability.

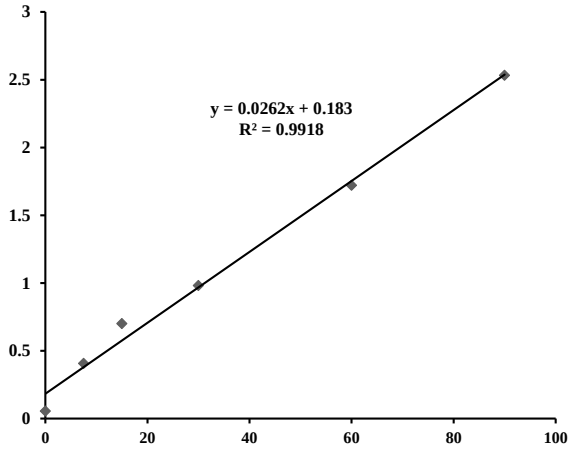


FIGURE 4.4: Standard curve generated for the quantification TNF-$\alpha$ by using ELISA.

It displays a clear linear relationship between the known concentrations of TNF-$\alpha$ (x-axis) and the corresponding optical density (OD) readings (y-axis). The regression equation ($y = 0.0262x + 0.183$) and the coefficient of determination ($R^2 = 0.9918$) indicate excellent linearity and a strong correlation between concentration and absorbance within the tested range.

In the control group, TNF-$\alpha$ concentration ranged between 7.90 and 9.42 $\mu$g/ml, reflecting the baseline inflammatory status in normal hippocampal tissue. However, scopolamine administration, which induces AD like neurodegeneration, led to a significant elevation in TNF-$\alpha$ level, with concentrations measured at 11.83 and 14.73 $\mu$g/ml. This increase indicates an intensified inflammatory response in the hippocampus, consistent with known mechanisms of neuroinflammation observed in Alzheimer's pathology. Treatment with donepezil in mice resulted in a broad range of TNF-$\alpha$ concentrations (10.07 to 14.50 $\mu$g/ml). Although there was some reduction compared to the peak scopolamine values, the cytokine levels in this group remained elevated compared to controls, suggesting that donepezil provides only partial protection against scopolamine-induced inflammation. The group treated with MBT at 5 mg/Kg demonstrated more favorable outcomes. TNF-$\alpha$ concentration in this group ranged from 12.17 to 13.01 $\mu$g/ml, with a slightly more consistent and reduced inflammatory profile compared to the donepezil group. This suggests that MBT at low doses may begin to exert anti-inflammatory effects, potentially through antioxidant or cytokine-modulating mechanisms. Notably, treatment with MBT at 10 mg/Kg produced even greater improvements. TNF-$\alpha$ concentration in this group ranged from 8.77 to 11.22 $\mu$g/ml, including one sample that nearly matched control levels. This indicates a dose-dependent anti-inflammatory effect of MBT, with the higher dose significantly attenuating the scopolamine-induced elevation in TNF-$\alpha$.

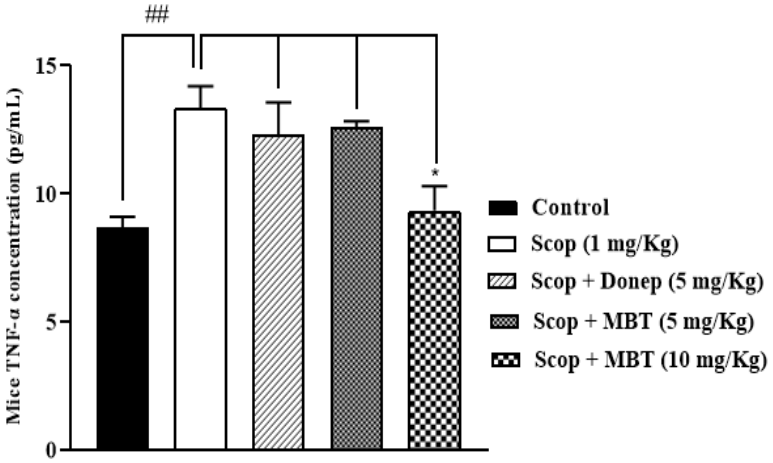


FIGURE 4.5: Effect of treatments on TNF-$\alpha$ level in mice hippocampus measured by ELISA.

Scopolamine (1 mg/Kg, i.p.) was administered once daily for 7 consecutive days to induce memory impairment and hippocampal neuroinflammation. MBT was administered intraperitoneally at doses of 5 mg/Kg and 10 mg/Kg, 30 minutes before scopolamine injection. Donepezil (1 mg/Kg, i.p.) was used as a reference drug. On day 8, animals were euthanized, and hippocampal tissues were collected for biochemical evaluation. TNF-$\alpha$ levels were quantified using ELISA to assess the inflammatory status. Results are expressed as mean ± SEM. Data indicate that MBT treatment, particularly at the 10 mg/Kg dose, significantly attenuated TNF-$\alpha$ expression in the hippocampus compared to the scopolamine group, suggesting a dose-dependent anti-inflammatory and neuroprotective effect. Statistical significance is denoted by *p $<$ 0.05, **p $<$ 0.01 vs. scopolamine group.

### 4.3.2 Interleukin-1 Beta

Interleukin-1 beta (IL-1$\beta$) levels in the hippocampal region were quantitatively assessed using enzyme-linked immunosorbent assay (ELISA). The standard curve established with serial concentrations of IL-1$\beta$ (90, 60, 30, 15, 7.5, and 0 $\mu$g/ml) yielded corresponding absorbance readings of 2.532, 1.721, 0.981, 0.7011, 0.407, and 0.055 respectively, confirming the sensitivity and linearity of the assay across the tested concentration range.

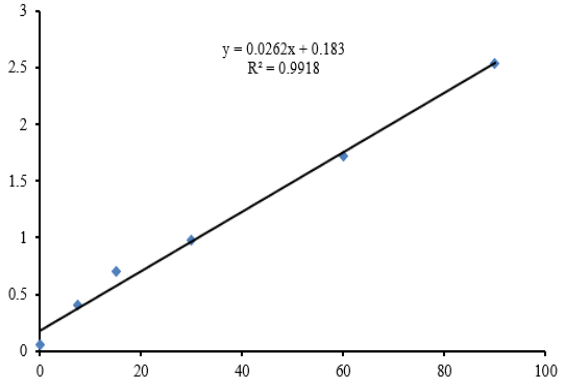


FIGURE 4.6: Standard curve generated for the quantification IL-1$\beta$ using ELISA.

It displays a clear linear relationship between the known concentrations of IL-1$\beta$ (x-axis) and the corresponding optical density (OD) readings (y-axis). The regression

equation (y = 0.0262x + 0.183) and the coefficient of determination ($R^2 = 0.9918$) indicate excellent linearity and a strong correlation between concentration and absorbance within the tested range.

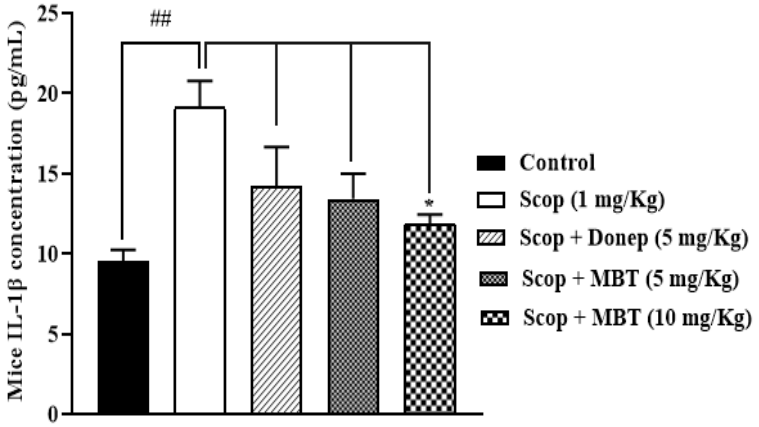


FIGURE 4.7: Effect of treatments on IL-1$\beta$ levels in mice hippocampus as measured by ELISA.

Scopolamine (1 mg/Kg, i.p.) was administered once daily for 7 consecutive days to induce memory impairment and hippocampal neuroinflammation. MBT was administered intraperitoneally at doses of 5 mg/Kg and 10 mg/Kg, 30 minutes before scopolamine injection. Donepezil (5 mg/Kg, p.o) was used as a reference drug. On day 8, animals were euthanized by cervical dislocation, and hippocampal tissues were collected for biochemical evaluation. IL-1 $\beta$ levels were quantified using ELISA to assess the inflammatory status. Results are expressed as mean ± SEM. Data indicate that MBT treatment, particularly at the 10 mg/Kg dose, significantly attenuated IL-1 $\beta$ expression in the hippocampus compared to the scopolamine group, suggesting a dose-dependent anti-inflammatory and neuroprotective effect. Statistical significance is denoted by *p $< 0.05$ vs. scopolamine group.

In the control group, IL-1$\beta$ concentrations ranged between 10.72 and 13.39 $\mu$g/ml, representing the physiological baseline level of this pro-inflammatory cytokine within healthy hippocampal tissue. Upon administration of scopolamine, which is known to induce Alzheimer's disease-like pathology, IL-1$\beta$ levels increased significantly. Specifically, concentrations reached 14.73 and 22.21 $\mu$g/ml, indicating a substantial elevation in hippocampal inflammation, particularly evident in the sample that recorded the highest cytokine level. This pronounced rise underscores the activation

of neuroinflammatory pathways commonly associated with neurodegeneration in AD models.

Interestingly, treatment with donepezil in mice resulted in IL-1$\beta$ concentrations of 10.89 and 18.93 $\mu$g/ml. These values suggest a partial normalization of IL-1$\beta$ levels compared to the scopolamine group, indicating that donepezil may exert some anti-inflammatory effects in addition to its primary role as an acetylcholinesterase inhibitor. However, the cytokine levels in the donepezil group still remained elevated compared to the lower end of the control range, reflecting incomplete suppression of the inflammatory response.

Administration of MBT at 5 mg/Kg led to IL-1$\beta$ concentrations between 15.99 and 17.09 $\mu$g/ml. While this represents an improvement over the elevated scopolamine levels, the values remain moderately high, suggesting that at this lower dose, MBT exerts only a limited anti-inflammatory effect. However, treatment with MBT at 10 mg/Kg resulted in further reductions, with IL-1$\beta$ concentrations recorded at 14.61 and 15.49 $\mu$g/ml. These values, while still above control levels, were lower than those observed in the 5 mg/Kg MBT group, suggesting a dose-dependent amelioration of hippocampal inflammation apoptotic, or synaptogenic mechanisms beyond cholinesterase inhibition.

TABLE 4.1: Total protein concentration ($\mu$g/ml) in hippocampus region of mice brain

| **Group** | **Protein Concentration ($\mu$g/ml)** | **Interpretation** |
|---|---|---|
| Control | 10.12 – 17.75 | Normal hippocampal function and protein integrity |
| Scopolamine | 7.24 – 10.30 | Protein loss due to neurodegeneration and synaptic impairment |
| Donepezil | 10.40 – 13.73 | Partial recovery via cholinesterase inhibition |
| MBT (5 mg/Kg) | 9.38 – 17.40 | Moderate, dose-dependent protection; some samples near control levels |
| MBT (10 mg/Kg) | 13.91 – 17.47 | Robust protein restoration; superior to donepezil and comparable to control |

## 4.4 Effects of MBT on Neuronal Survival Assessed by Hematoxylin and Eosin Staining

The hippocampus plays a crucial role in learning and memory and is particularly vulnerable in AD. Histopathological evaluation allows the assessment of therapeutic efficacy at a cellular level by examining neuronal integrity, glial activation, and neurovascular changes. In this study, hippocampal sections were analyzed to compare the effects of MBT at two different doses against a scopolamine-induced neurodegenerative model. The H&E staining is one of the most widely used techniques in histopathology for evaluating the general morphology and cellular architecture of tissue sections. In this method, hematoxylin, a basic dye, binds strongly to nucleic acids and stains cell nuclei a deep blue to purple color. This nuclear staining enables detailed visualization of nuclear morphology, including chromatin condensation, nuclear fragmentation, and hallmarks of neurodegeneration. The MBT 10 mg/Kg group displays preserved neuronal architecture with intact and organized hippocampal structure, indicating strong neuroprotection. The MBT 5 mg/Kg group shows moderate neuronal preservation, with partial attenuation of degenerative changes. In the scopolamine (1 mg/Kg) group, severe neurodegenerative features are evident, including disrupted architecture, reduced neuronal density, and numerous pyknotic neurons. The control group exhibits normal hippocampal morphology with tightly packed and orderly arranged neurons These findings suggest a dose-dependent neuroprotective effect of MBT in mitigating scopolamine-induced hippocampal damage.

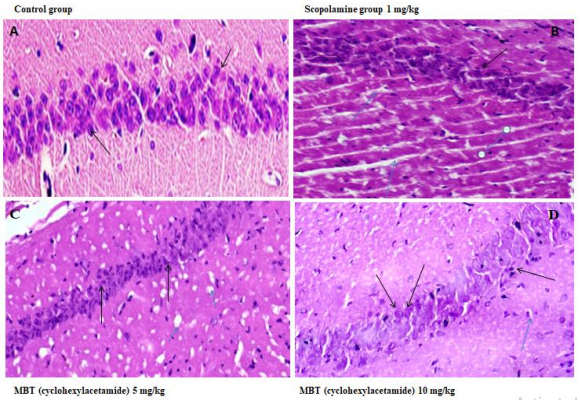


FIGURE 4.8: Hematoxylin and eosin (H&E) stained coronal sections from the CA1 region of the hippocampus at 10x magnification.

The above figure shows the histopathological evaluation of hematoxylin and eosin (H&E)-stained coronal sections from the CA1 region of the hippocampus (scale bar: 25 $\mu$m) revealed distinct morphological differences among treatment groups. In the control group (A), the hippocampal architecture appeared normal, with densely packed, well-organized pyramidal neurons (indicated by black arrows), reflecting intact neuronal integrity. In contrast, the scopolamine-treated group (1 mg/kg) (B) exhibited significant neurodegenerative changes, including extensive neuronal loss, disorganization of pyramidal cell layers, pyknotic nuclei, and widespread vacuolation (blue arrows), along with compromised neuronal morphology (black arrow). These alterations are indicative of pronounced scopolamine-induced neurotoxicity. Administration of MBT (cyclohexylacetamide) at a dose of 5 mg/kg (C) resulted in partial neuroprotection, as evidenced by moderately preserved neuronal arrangements and reduced vacuolation (blue arrows), while black arrows denote signs of neuronal regeneration. Notably, treatment with a higher dose of MBT (10 mg/kg) (D) led to substantial preservation of hippocampal structure, with minimal vacuolation (blue arrows) and restored neuronal morphology (black arrows), closely resembling the control group. These findings demonstrate a clear dose-dependent neuroprotective effect of MBT against scopolamine-induced hippocampal damage.

## 4.5 Molecular Docking Analysis with MBT Compound at Different Cytokines Receptors

Among the tested ligands, cyclohexylactamide demonstrated the highest docking score compared to Morpholine and Octylamine, indicating a relatively stronger binding affinity. However, all the ligands exhibited lower docking scores than the reference compound, Donepezil, suggesting that while they form stable complexes with IL-1$\beta$, they are less potent than the standard. The docking scores of the three ligands were -5.9 kcal/mol, -5.6 kcal/mol, and -5.1 kcal/mol, respectively, compared to Donepezil's -7.7 kcal/mol.

TABLE 4.2: The energy score for the ligand against IL-1$\beta$

| Sr. No | Target protein | PDB ID | Ligand | Docking score |
|---|---|---|---|---|
| **1** | IL-1$\beta$ | 8c3u | Cyclohexylactamide | -5.9 |
| **2** | IL-1$\beta$ | 8c3u | Morpholine | -5.6 |
| **3** | IL-1$\beta$ | 8c3u | Octylamine | -5.1 |

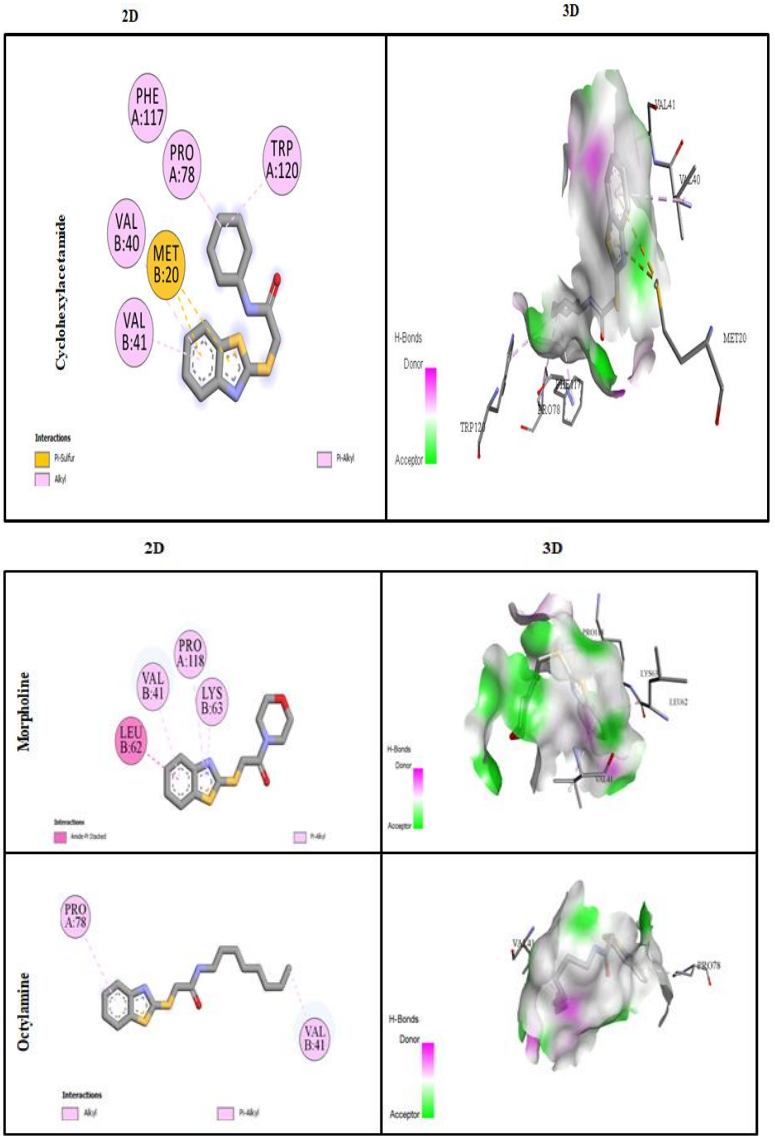


The 2D interaction diagram of cyclohexylacetamide bound to the target protein reveals

several important non-covalent interactions that contribute to the stability and affinity of the ligand within the binding pocket. Notably, a $\pi$-sulfur interaction is observed between the aromatic ring of cyclohexylacetamide and the sulfur atom of Methionine (MET B:20), which plays a crucial role in stabilizing the complex through hydrophobic effects. In addition, alkyl interactions are evident with Valine residues (VAL B:40 and VAL B:41), where the non-polar alkyl chains of these amino acids interact with the hydrophobic cyclohexyl group of the ligand. These interactions enhance van der Waals forces and contribute to the overall binding strength. Furthermore, $\pi$-alkyl interactions are formed with Proline (PRO A:78), Phenylalanine (PHE A:117), and Tryptophan (TRP A:120). These interactions involve the $\pi$-electron cloud of the ligand's aromatic ring engaging with the alkyl side chains or cyclic rings of the respective amino acids, further stabilizing the ligand within the active site. Collectively, these hydrophobic and $\pi$-electron interactions form a robust binding environment, despite the absence of classical hydrogen bonds. The positioning of Cyclohexylacetamide in this hydrophobic pocket and the diverse interaction profile underscore its potential as a moderately strong binder, and provide valuable insights for structural optimization in future drug design efforts.

### 4.5.1 Tumor Necrosis Factor Alpha

Cyclohexylactamide again emerged as the ligand with the highest docking score (-7.7 kcal/mol), followed closely by Morpholine (-7.6 kcal/mol), and Octylamine (-6.6 kcal/mol). All three ligands showed slightly lower affinity compared to Donepezil (-8.7 kcal/mol), indicating that while these ligands may form moderately stable complexes with TNF-$\alpha$, Donepezil remains superior in terms of binding efficiency (Table 4.3).

TABLE 4.3: The energy score for the ligand against TNF-$\alpha$

| **Sr. No** | **Target protein** | **PDB ID** | **Ligand** | **Docking score** |
|---|---|---|---|---|
| 1 | TNF-$\alpha$ | 7jra | Cyclohexylactamide | -7.7 |
| 2 | TNF-$\alpha$ | 7jra | Morpholine | -7.6 |
| 3 | TNF-$\alpha$ | 7jra | Octylamine | -6.6 |

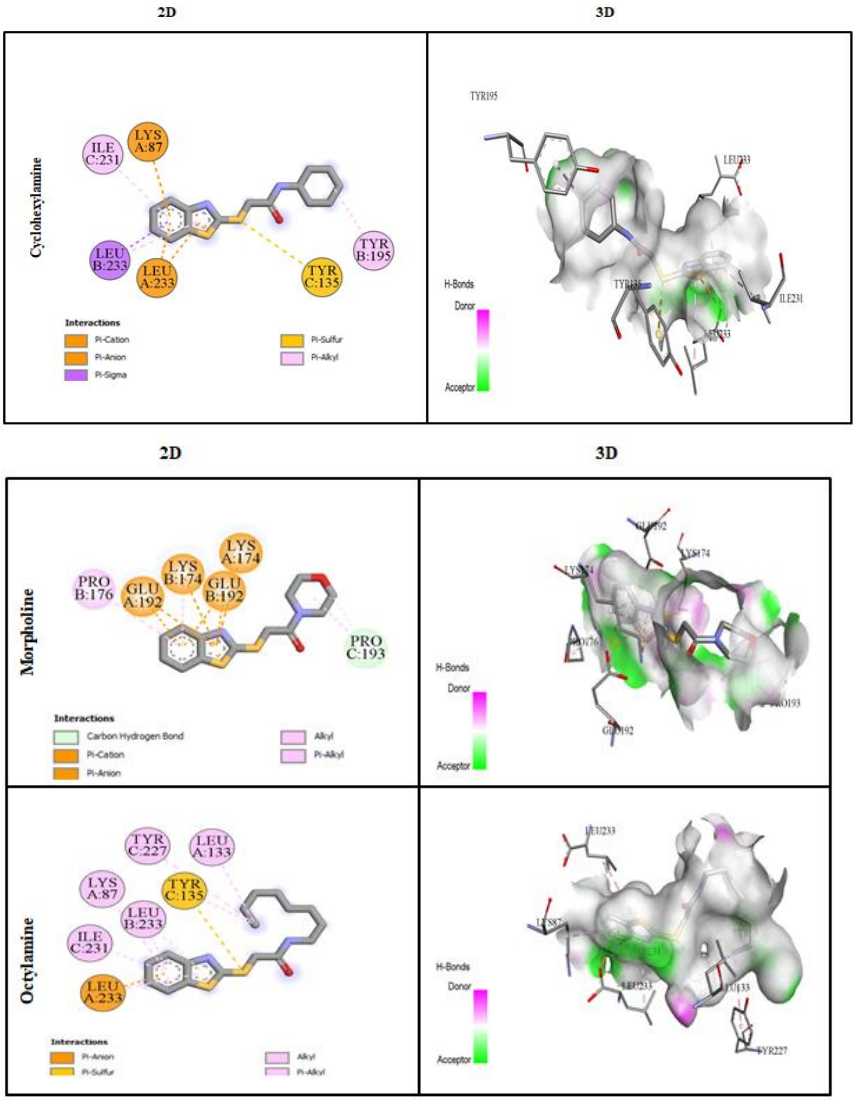


The 2D interaction diagram of cyclohexylacetamide with the selected target protein reveals a diverse array of non-covalent interactions that collectively contribute to a stable ligand-protein complex. A prominent feature is the presence of multiple $\pi$-alkyl interactions, involving Tyrosine (TYR B:195 and TYR C:135), Leucine (LEU A:233), and Isoleucine (ILE C:231). These interactions occur between the $\pi$-electron cloud of the aromatic ring in the ligand and the hydrophobic side chains of the respective amino acids, enhancing the overall hydrophobic stabilization within the binding pocket. Additionally, a $\pi$-sulfur interaction is observed with Tyrosine (TYR C:135), where the aromatic ring interacts with the sulfur-containing side chain, contributing to the ligand's affinity through favorable dispersion forces. The diagram also shows a significant $\pi$-anion interaction with Leucine (LEU

B:233), although leucine is not typically an anionic residue; this could indicate an environment influenced by nearby acidic residues or electrostatic contributions in the binding site. Moreover, a $\pi$-cation interaction is seen with Lysine (LYS A:87), where the positively charged ammonium side chain of lysine forms an electrostatic attraction with the aromatic system of the ligand. This interaction is particularly important in anchoring the ligand via strong ionic forces. Lastly, a $\pi$-sigma interaction with Leucine (LEU A:233) is noted, providing additional stabilization through orbital overlap between the $\pi$-system and the sigma bonds of adjacent residues.

### 4.5.2 Nuclear Factor Kappa

In the case of NF-$\kappa$B, cyclohexylactamide once more showed the highest docking score among the test ligands, with a value of -5.5 kcal/mol. Morpholine and Octylamine followed closely with scores of -5.4 kcal/mol and -4.1 kcal/mol, respectively. As observed in previous results, all ligands showed lower binding affinities than donepezil (-7.0 kcal/mol), reinforcing donepezil's superior performance as a standard inhibitor (Table 4.4)

Table 4.4: The energy score for the ligand against NF-$\kappa$B

| Sr. No | Target protein | PDB ID | Ligand | Docking score |
|---|---|---|---|---|
| 1 | NF-$\kappa$B | 9bdw | Cyclohexylactamide | -5.5 |
| 2 | NF-$\kappa$B | 9bdw | Morpholine | -5.4 |
| 3 | NF-$\kappa$B | 9bdw | Octylamine | -4.1 |

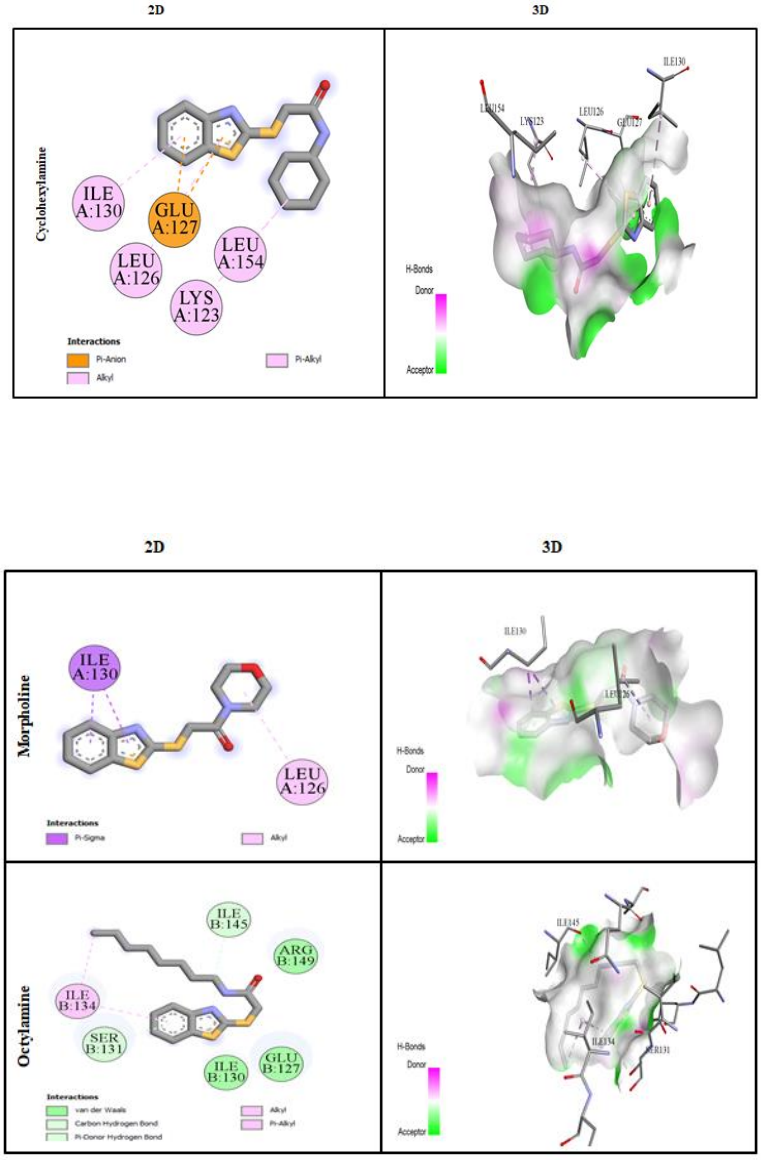


The 2D interaction diagram of cyclohexylacetamide with the target protein highlights several key interactions that contribute to the stabilization of the ligand within the active site. A prominent $\pi$-anion interaction is observed between the aromatic ring of cyclohexylacetamide and the negatively charged side chain of Glutamic acid (GLU A:127). This interaction is significant, as the electrostatic attraction between the $\pi$-electron cloud of the aromatic ring and the anionic carboxylate group enhances the binding affinity. Additionally, alkyl interactions are noted with Leucine (LEU A:126 and LEU A:154) and Lysine (LYS A:123) residues. These hydrophobic contacts involve the interaction between the ligand's non-polar cyclohexyl moiety and the side chains of the hydrophobic amino acids, promoting

van der Waals forces that contribute to ligand stabilization. Moreover, $\pi$-alkyl interactions are seen with Isoleucine (ILE A:130) and Leucine (LEU A:126), where the $\pi$-system of the aromatic ring interacts favorably with the alkyl side chains of these residues. These $\pi$-alkyl interactions further reinforce the hydrophobic nature of the binding pocket. Overall, the ligand is well accommodated within a predominantly hydrophobic and partially charged environment, where $\pi$-anion and hydrophobic interactions work synergistically to support a moderately stable ligand-protein complex.

TABLE 4.5: Molecular interactions of MBT (cyclohexylacetamide) with target inflammatory proteins (IL-1$\beta$, TNF-$\alpha$, and NF-$\kappa$B) based on docking analysis

| **Target Protein** | **Interacting Residue(s)** | **Interaction Type** | **Interaction Nature** |
|---|---|---|---|
| IL-1$\beta$ (PDB ID: 8c3u) | MET B:20 | $\pi$–Sulfur | Hydrophobic |
| | VAL B:40, VAL B:41 | Alkyl | Hydrophobic |
| | PRO A:78, PHE A:117, TRP A:120 | $\pi$–Alkyl | Hydrophobic |
| TNF-$\alpha$ (PDB ID: 7jra) | TYR B:195, TYR C:135 | $\pi$–Alkyl/ $\pi$–Sulfur | Hydrophobic |
| | LEU A:233, ILE C:231 | Alkyl / $\pi$–Alkyl | Hydrophobic |
| | LYS A:87 | $\pi$–Cation | Hydrophilic (electrostatic) |
| | LEU B:233 (via local acidic environment) | $\pi$–Anion | Hydrophilic (electrostatic) |
| NF-$\kappa$B (PDB ID: 9bdw) | GLU A:127 | $\pi$–Anion | Hydrophilic (electrostatic) |
| | LEU A:126, LEU A:154 | Alkyl | Hydrophobic |
| | LYS A:123 | Alkyl | Hydrophobic |
| | ILE A:130 | $\pi$–Alkyl | Hydrophobic |

## 4.6 In *Silico* Toxicity Studies

The *in silico* toxicity evaluation of MBT derivative (Cyclohexylactamide) was conducted using ToxTree software based on the Cramer classification scheme. The compound was classified under Cramer Class III (High Toxicity), indicating a high level of concern for potential systemic toxicity. The stepwise decision tree output showed that MBT did not satisfy several criteria associated with low or intermediate toxicity classes. Specifically, the compound was flagged for containing

a heterocyclic ring with complex substituents (Rule Q11), a structural feature commonly associated with increased toxicological potential.

Other criteria such as the presence of non-standard functional groups, lack of simple hydrocarbon structure, and structural complexity contributed to its classification into the highest hazard category. The potential oral toxicity of the compound MBT derivative (Cyclohexylactamide) was evaluated using the ProTox-II platform, an advanced computational tool that predicts toxicity based on chemical structure similarity, molecular descriptors, and machine learning algorithms. The analysis yielded a predicted median lethal dose (LD50) of 1077 mg/Kg body weight, suggesting that the compound exhibits moderate acute oral toxicity.

Based on the Globally Harmonized System classification employed by ProTox-II, MBT falls under Toxicity Class 4, which includes substances with LD50 values ranging between 300 and 2000 mg/Kg. Compounds in this category are considered harmful if ingested and may present moderate risk at higher doses.

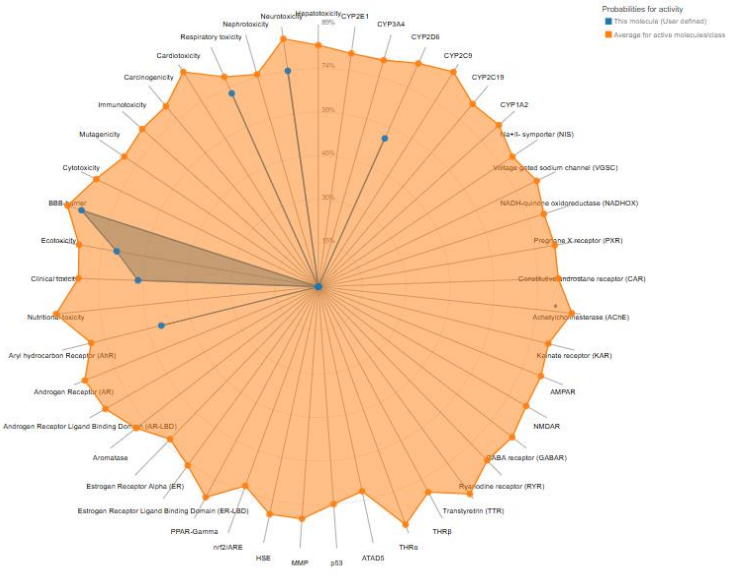


FIGURE 4.9: Toxicity radar chart

The radar chart predicted toxicological and pharmacological profile of cyclohexylacetamide across multiple endpoints relevant to drug safety and central nervous system (CNS) activity. Each axis represents a distinct biological target or toxicological parameter, with the distance from the center corresponding to the predicted

probability of activity. The blue points indicate specific predictions for cyclohexylacetamide, while the orange shaded area represents average profiles for known active substances in each category. The compound displays low predicted risks for immunotoxicity, mutagenicity, carcinogenicity, cytotoxicity, and clinical toxicity, supporting its safety for in vivo applications. Importantly, moderate blood–brain barrier (BBB) permeability was observed, which is a favorable feature for CNS-targeted therapies, such as those intended for the treatment of Alzheimer's disease (AD). This aligns well with our study's focus on evaluating neuroprotective effects in a scopolamine-induced AD mouse model. Additionally, cyclohexylacetamide showed minimal interaction with key neurotransmitter receptors (NMDA, GABA,), suggesting that it is unlikely to disrupt essential synaptic functions or contribute to excitotoxicity. This is particularly relevant to AD pathology, where excitotoxic mechanisms and cholinergic deficits play a major role. The compound also exhibited low hepatotoxicity and cardiotoxicity potential, indicating systemic safety upon chronic administration. The absence of ecotoxicity and reproductive toxicity predictions further enhances the compound's safety profile. Taken together, these in silico results reinforce the experimental findings of our study, in which cyclohexylacetamide treatment preserved hippocampal integrity and improved cognitive performance in mice. The radar chart thus complements and validates the compound's potential as a safe and effective neuroprotective agent for further development in AD therapeutics.

# Chapter 5

# Discussion of Studies

The present study evaluated the acute toxicity profile of the test compound MBT through both *in vivo* and *in silico* approaches, providing a comprehensive assessment of its safety and potential risks.

## 5.1 In *Vivo* Acute Toxicity Assessment

In vivo toxicity evaluation was conducted using a murine model, where a single dose of 100 mg/Kg body weight of MBT was administered. The results demonstrated that at this concentration, the compound did not induce any observable adverse behavioral responses, nor did it cause significant changes in body weight or mortality over the observation period.

These findings suggest that MBT at this dosage is well-tolerated in mice and can be considered safe for further pharmacological investigations, including its anti-inflammatory potential in AD models.

Similar studies have shown that compounds with comparable doses and exposure routes exhibit minimal toxicity in rodent models. Such a safety profile is encouraging, particularly given the need for compounds with minimal toxicity in the development of therapeutic agents for neurodegenerative diseases.

## 5.2 In *Silico* Toxicity Predictions

To complement the *in vivo* studies, computational toxicity assessments were conducted to evaluate the potential systemic hazards of MBT compound particularly cyclohexylactamide. ToxTree analysis classified cyclohexylactamide in Cramer Class III, suggesting a high potential for systemic toxicity due to its complex heterocyclic structure and substituents, which are commonly associated with increased toxicological risks. Additionally, ProTox-II predicted an oral LD50 of 1077 mg/Kg, categorizing the compound under GHS Toxicity Class 4 indicating moderate acute toxicity. These findings highlight the need for cautious dose consideration in future therapeutic development. The toxicity studies reinforce MBT's potential as a relatively safe compound for continued research, providing a foundation for its further evaluation in anti-inflammatory and neuroprotective contexts. However, comprehensive long-term toxicity assessments and dose optimization remain essential to ensure safety in eventual clinical applications.

The behavioral assessments conducted in this study, including the MWM and Y-maze tests, provide compelling evidence for the potential therapeutic efficacy of the MBT compound in mitigating scopolamine-induced spatial and working memory deficits, a well-established model of AD like cognitive impairment. The findings underscore the ability of MBT to ameliorate memory dysfunction, aligning with the behavioral outcomes observed with donepezil, a clinically approved acetylcholinesterase inhibitor used as a positive control in this study.

## 5.3 Comparative Behavioral Assessment in Morris Water Maze and Y-Maze Test

In the MWM test, scopolamine administration significantly prolonged escape latency and reduced the time spent in the target quadrant during the probe trial, indicative of impaired spatial learning and memory consolidation. These results are consistent with prior studies demonstrating that scopolamine, a muscarinic cholinergic receptor

antagonist, disrupts hippocampal dependent memory processes by interfering with acetylcholine signaling a critical neurotransmitter for synaptic plasticity and memory formation. Notably, pretreatment with MBT (5 or 10 mg/Kg) attenuated these deficits, as evidenced by the dose-dependent reduction in escape latency and increased target quadrant exploration. The efficacy of MBT at both doses paralleled that of donepezil, suggesting its potential to modulate cholinergic pathways or enhance compensatory mechanisms to counteract scopolamine-induced deficits. The significant improvement in probe trial performance further supports MBT's role in preserving long-term spatial memory, likely by mitigating hippocampal dysfunction or oxidative stress, common contributors to AD pathology.

Complementary findings from the Y-maze test reinforced these observations. Scopolamine-treated mice exhibited a marked decline in spontaneous alternation behavior, reflecting impaired working memory and reduced exploratory drive. This deficit aligns with the role of acetylcholine in sustaining attention and short-term memory processes. However, MBT pretreatment restored spontaneous alternation to near-normal levels, with the higher dose (10 mg/Kg) eliciting a robust response comparable to donepezil. The Y-maze results collectively highlight MBT's capacity to enhance cognitive flexibility and working memory, further supporting its neuroprotective potential in AD model. The consistency of MBT's effects across both behavioral paradigms MWM (hippocampal-dependent spatial memory) and Y-maze (prefrontal cortex-mediated working memory) suggests a broad-spectrum neuroprotective action. This could involve modulation of cholinergic transmission, anti-inflammatory properties, or antioxidant effects, all of which are implicated in AD progression. The dose-dependent response observed in both tests further validates the compound's pharmacological relevance and underscores the importance of optimizing dosing regimens for therapeutic translation.

While the current findings are promising, several considerations warrant further investigation. First, the exact mechanism by which MBT exerts its cognitive-enhancing effects remains to be elucidated. Future studies should explore its interaction with cholinergic receptors, amyloid-beta aggregation, or neuroinflammatory pathways. Second, the use of intraperitoneal administration for MBT versus

oral dosing for donepezil introduces variability in pharmacokinetic profiles, necessitating comparative bioavailability studies. In conclusion, this study demonstrates that the MBT compound effectively reverses scopolamine-induced cognitive deficits in mice, as evidenced by improvements in spatial navigation, memory retention, and working memory. These findings position MBT as a promising candidate for further preclinical development in AD therapeutics.

## 5.4 Comparative Evaluation of MBT on Hippocampal Protein Preservation in Mice

The BCA assay offered critical quantitative insights into hippocampal protein content across experimental groups in a scopolamine-induced AD mice model. The standard curve exhibited strong linearity ($R^2$=0.996), validating the assay's reliability and enabling accurate intergroup comparison. As presented in table 4, the control group exhibited consistently high protein concentrations (10.12–17.75 $\mu$g/ml), reflecting normal hippocampal function and protein integrity essential for synaptic maintenance and neuronal health. In contrast, the scopolamine-treated group displayed a significant reduction in hippocampal protein levels (7.24–10.30 $\mu$g/ml), consistent with scopolamine's neurotoxic effects that mimic AD pathology, including oxidative stress, synaptic degradation, and cholinergic deficits. Donepezil treatment partially ameliorated this protein loss, with concentrations ranging from 10.40 to 13.73 $\mu$g/ml. Although this reflects its neuroprotective efficacy via acetylcholinesterase inhibition and improved cholinergic transmission, the incomplete recovery indicates its limitations in counteracting multifaceted neurodegeneration. Treatment with MBT showed a clear dose-response trend. The 5 mg/Kg dose exhibited a wider and less consistent range (9.38–17.40 $\mu$g/ml), suggesting moderate efficacy with some samples approximating control values. Remarkably, the 10 mg/Kg MBT group achieved highly consistent and elevated protein concentrations (13.91–17.47 $\mu$g/ml), closely mirroring the control group This suggests that MBT exerts more comprehensive neuroprotective effects, potentially involving antioxidative, anti-inflammatory and neuroprotective compound. The

findings strongly indicate that MBT, particularly at 10 mg/Kg, offers significant neuroprotection in the scopolamine-induced AD model, as evidenced by maximum restoration of hippocampal protein levels. It has a broader therapeutic mechanism, possibly involving modulation of oxidative stress and synaptic preservation. These results support the continued investigation of MBT as a multi-target candidate for AD treatment.

## 5.5 Neuroprotective and Anti-Inflammatory Potential of MBT in a Scopolamine-Induced Model of Alzheimer's Disease

Neuroinflammation is a central pathological feature in AD, often driven by overexpression of pro-inflammatory cytokines such as TNF-$\alpha$ and IL-1$\beta$. The current study assessed the anti-inflammatory potential of MBT in a scopolamine-induced mouse model of AD by quantifying hippocampal levels of TNF-$\alpha$ and IL-1$\beta$ via ELISA. The findings offer compelling evidence for the neuroprotective role of MBT, particularly at the higher 10 mg/Kg dose, with superior efficacy. Scopolamine administration elicited a marked upregulation of TNF-$\alpha$ and IL-1$\beta$ in hippocampal tissues, affirming its role in inducing a robust inflammatory phenotype that mimics aspects of AD neuropathology. The TNF-$\alpha$ concentration peaked between 11.83 and 14.73 $\mu$g/ml, significantly exceeding control values (7.90–9.42 $\mu$g/ml). This elevation is indicative of activated microglial response and cytokine-mediated neurotoxicity, processes known to impair synaptic signaling and promote neuronal apoptosis in AD. Similarly, IL-1$\beta$ levels rose dramatically following scopolamine exposure, with concentrations up to 22.21 $\mu$g/nearly double the upper range of the control group (10.72–13.39 $\mu$g/ml). This sharp increase in IL-1$\beta$ pivotal role in amplifying the inflammatory milieu and perpetuating neurodegeneration. Donepezil-treated animals showed only partial attenuation of cytokine expression. While TNF-$\alpha$ levels (10.07–14.50 $\mu$g/ml) and IL-1$\beta$ levels (10.89–18.93 $\mu$g/ml) were lower than in the scopolamine group, they remained substantially elevated compared

to control. These results align with the pharmacological profile of donepezil as a cholinesterase inhibitor with minimal direct influence on pro-inflammatory cytokine pathways. Thus, while donepezil improves cognitive function through cholinergic enhancement, its capacity to suppress neuroinflammation appears limited. The MBT treatment, in contrast, elicited a dose-dependent suppression of inflammatory cytokines. At 5 mg/Kg, MBT moderately decreased TNF-$\alpha$ levels (12.17–13.01 $\mu$g/ml) and IL-1$\beta$ levels (15.99–17.09 $\mu$g/ml), indicating the compound's ability to interfere with inflammatory cascades. The improved consistency of cytokine levels in this group compared to donepezil further suggests that MBT may possess intrinsic anti-inflammatory properties. The 10 mg/Kg MBT group demonstrated significantly greater anti-inflammatory activity. TNF-$\alpha$ concentrations (8.77–11.22 $\mu$g/ml) closely approached the control range, with one value nearly overlapping, suggesting near complete reversal of scopolamine-induced cytokine induction. Similarly, IL-1$\beta$ levels (14.61–15.49 $\mu$g/ml), though still mildly elevated, were lower than those seen in both the 5 mg/Kg MBT and donepezil groups, reinforcing the dose-response relationship. These findings support the hypothesis that MBT confers neuroprotection not only via cholinergic pathways but also by modulating neuroinflammation. MBT's suppression of pro-inflammatory cytokines may stem from its potential to scavenge reactive oxygen species, inhibit NF-$\kappa$B signaling, or stabilize glial cell activity mechanisms increasingly recognized in the context of AD therapeutics.

For H&E staining the findings of this study demonstrate that the MBT compound (cyclohexylacetamide) effectively protects the brain from damage in a mouse model of Alzheimer's like memory impairment. By analyzing hippocampal tissue the brain region crucial for memory, we observed that MBT reduces structural harm caused by scopolamine, a drug used to mimic AD pathology. In healthy mice, the hippocampus displayed tightly packed, well-organized brain cells, reflecting normal brain structure. However, mice treated with scopolamine showed severe neuronal damage, including cell loss, disorganized layers, and shrunken, dying cells, mirroring the neurodegeneration seen in Alzheimer's disease Treatment with MBT at a lower dose (5 mg/Kg) partially reversed this damage, improving cellular organization and reducing signs of cell death, though some degenerative features persisted. At

the higher dose (10 mg/Kg), MBT nearly restored the hippocampus neurons to its healthy state, with intact neuronal layers and minimal damage, highlighting its dose-dependent neuroprotective effects. These structural improvements align with earlier behavioral tests, where MBT improved memory in tasks like the Morris Water Maze and Y-maze. The stronger structural preservation seen at the higher dose likely explains the more robust memory recovery, connecting healthier brain tissue directly to better cognitive function. While the exact mechanisms remain unclear, MBT's benefits may stem from its ability to combat oxidative stress (neutralizing harmful molecules that damage cells), reduce inflammation (calming brain inflammation that worsens neurodegeneration), or support brain cell survival by stabilizing cell membranes or enhancing energy production. However, further research is needed to confirm these pathways. A key limitation of this study is its reliance on scopolamine, which induces acute damage rather than mimicking the slow progression of AD. In conclusion, MBT emerges as a promising candidate for mitigating Alzheimer's-related brain damage by preserving hippocampal structure and function, it offers a dual benefit of protecting neurons and restoring memory. Though more work is needed to unravel its mechanisms and validate its use in realistic disease models, these findings provide a hopeful foundation for developing therapies that could slow or prevent the devastating brain changes seen in AD.

Molecular docking analysis serves as a vital tool in rational drug design, offering insights into the binding conformation, affinity, and interaction profile of bioactive compounds within protein targets. In the current study, MBT was evaluated for its binding potential against three critical pro-inflammatory mediators Interleukin-1$\beta$ (IL-1$\beta$), Tumor Necrosis Factor-alpha (TNF-$\alpha$), and Nuclear Factor-kappa B (NF-$\kappa$B). These targets are well-recognized for their pivotal roles in neuroinflammation and the progression of AD. Cyclohexylactamide consistently exhibited the highest docking scores among the test ligands (including morpholine and octylamine), indicating a favorable binding affinity. However, all test compounds displayed lower binding energies compared to the reference standard Donepezil, reflecting the latter's established potency as a clinically validated cholinesterase inhibitor with additional anti-inflammatory properties. In the IL-1$\beta$ cyclohexylactamide complex, a docking score of 5.9 kcal/mol was recorded. The interaction profile revealed

strong stabilization within the hydrophobic core of the binding pocket, primarily via $\pi$–sulfur interaction with MET B:20, alkyl interactions with VAL B:40 and VAL B:41, and multiple $\pi$–alkyl contacts with aromatic residues such as PRO A:78, PHE A:117, and TRP A:120. These interactions suggest that the compound's cyclohexyl and aromatic moieties are well accommodated within the nonpolar pocket of IL-1$\beta$, promoting van der Waals and dispersion forces essential for ligand retention. Against TNF-$\alpha$, cyclohexylactamide demonstrated a more favorable binding energy of –7.7 kcal/mol. The interaction map highlighted a combination of hydrophobic contacts—$\pi$–alkyl and $\pi$–sulfur interactions with TYR B:195 and TYR C:135, along with LEU A:233 and ILE C:231 and notable electrostatic interactions, including a $\pi$–cation interaction with LYS A:87 and a $\pi$–anion interaction involving LEU B:233 (likely mediated by nearby acidic residues). These findings suggest that the ligand's binding within TNF-$\alpha$ is not only governed by hydrophobic packing but also reinforced by selective polar contacts, enhancing overall complex stability.

In the NF-$\kappa$B complex, cyclohexylactamide yielded a docking score of –5.5 kcal/mol. Although lower than TNF-$\alpha$, the compound maintained favorable interactions including a $\pi$–anion interaction with GLU A:127, and hydrophobic alkyl and $\pi$ alkyl interactions with LEU A:126, LEU A:154, LYS A:123, and ILE A:130. The $\pi$ anion contact with glutamate may contribute significantly to the compound's anchoring within the active site, despite the generally lower binding affinity compared to other targets. Collectively, these results underscore the capacity of cyclohexylactamide to engage in a diverse spectrum of non-covalent interactions, stabilizing its orientation across multiple inflammatory targets. Its consistent performance suggests potential multi-target anti-inflammatory and neuroprotective effects, which may contribute to the observed *in vivo* efficacy. The molecular docking findings reveal that cyclohexylactamide forms energetically stable and structurally favorable complexes with pro-inflammatory cytokines through a combination of hydrophobic interactions and selective electrostatic contacts. These interactions collectively facilitate effective receptor binding, suggesting the potential of MBT as a lead compound for further development in anti-inflammatory and neuroprotective therapeutics. Future studies should focus on optimizing the functional groups of cyclohexylactamide to

enhance hydrogen bonding potential and receptor specificity. Additionally, molecular dynamics simulations and *in-vitro* assays involving cytokine inhibition and neuronal cell survival could provide further validation of its therapeutic promise in neuroinflammatory contexts such as AD.

# Chapter 6

# Conclusion and Future Work

## 6.1 Conclusion

The present study demonstrates the neuroprotective and anti-inflammatory effect of mercaptobenzothiazole (MBT) in a scopolamine-induced model of AD. Behavioral assessments using MWM and Y-maze tests, revealed statistically significant improvements in spatial and working memory following MBT administration. At the higher dose (10 mg/Kg), escape latency was reduced ($p < 0.001$) and spontaneous alternation behavior increased significantly ($p < 0.001$) compared to the scopolamine group, indicating robust cognitive enhancement.

The above diagram shows neuroprotective and anti-inflammatory effects of mercaptobenzothiazole (MBT) showing cognitive performance, as evidenced by improved spatial and working memory in behavioral assessments such as the Morris Water Maze (MWM) and Y-maze tests. These cognitive benefits are linked to MBT's neuroprotective and anti-inflammatory actions at the effective dose of 10 mg/kg. This central effect is further supported by reduced hippocampal levels of pro-inflammatory cytokines, specifically TNF-$\alpha$ and IL-1$\beta$, indicating significant suppression of neuroinflammation. Molecular docking analysis suggests that MBT favorably interacts with key inflammatory mediators including TNF-$\alpha$, IL-1$\beta$, and NF-$\kappa$B, contributing to the mechanistic understanding of its anti-inflammatory properties. Additionally, histopathological examination revealed better preservation

of hippocampal neuronal architecture in MBT-treated mice, indicating reduced neurodegeneration. Collectively, the diagram emphasizes the multi-targeted therapeutic potential of MBT in mitigating cognitive decline and inflammation associated with AD.

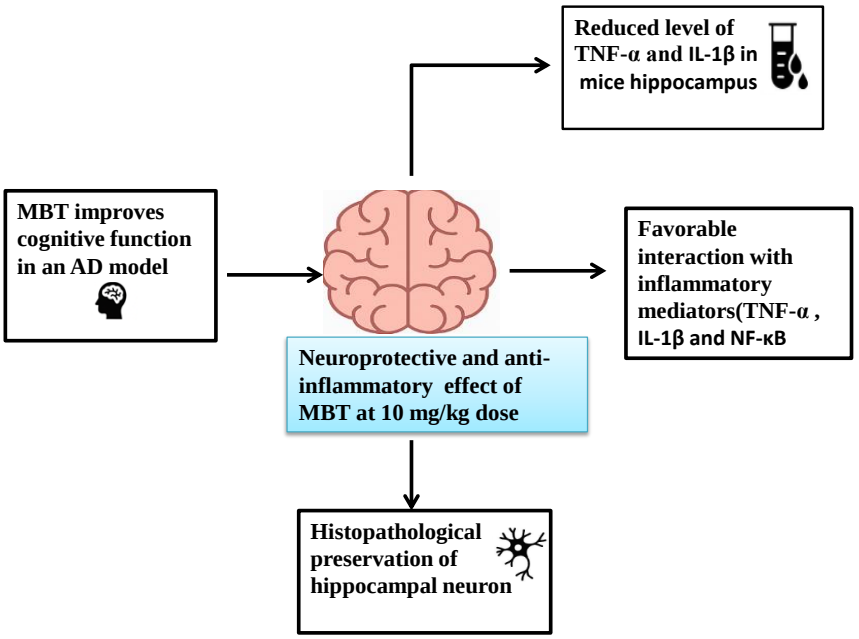


FIGURE 6.1: Graphical summary of MBT neuroprotective effects in an Alzheimer's disease (AD) model.

Biochemical analysis corroborated these findings, with MBT treatment significantly decreasing hippocampal levels of pro-inflammatory cytokines. Specifically, IL-1$\beta$ levels were reduced by ($p < 0.01$) and TNF-$\alpha$ levels by ($p < 0.05$) at the 10 mg/Kg dose relative to the scopolamine group, demonstrating dose-dependent anti-inflammatory activity. Histopathological examination of hippocampal sections further supported these outcomes, showing preserved neuronal architecture and reduced neurodegeneration in MBT-treated mice.

Molecular docking revealed favorable interactions of MBT with key inflammatory mediators, including TNF-$\alpha$, IL-1$\beta$, and NF-$\kappa$B, through stable hydrophobic and electrostatic binding, suggesting a plausible mechanistic basis for its observed effects. Acute toxicity profiling indicated that MBT was well-tolerated in vivo, although computational toxicity predictions suggest the need for caution regarding long-term systemic exposure.

MBT exhibits multi-target neurotherapeutic potential by concurrently attenuating neuroinflammation and improving cognitive function in an AD model. However, future investigations employing chronic and transgenic models, along with detailed pharmacokinetic and mechanistic studies, are warranted to validate and extend these promising findings toward clinical relevance.

## 6.2 Future Perspectives

To support the translational development of MBT as a novel therapeutic candidate for AD, future studies should adopt a multidisciplinary and mechanistically driven strategy. Expanding preclinical evaluations to transgenic AD mouse models (3xTg-AD, APP/PS1) and aged animal cohorts will be critical for assessing MBT's efficacy against hallmark AD pathologies such as amyloid-beta (A$\beta$) plaques and hyperphosphorylated tau aggregates, thereby validating its therapeutic potential in both acute and progressive disease contexts. BBB permeability studies will help determine MBT's central nervous system penetrance, a critical feature for neurotherapeutics. These chronic models will help determine whether MBT maintains its efficacy over time and whether it can modify disease progression rather than merely alleviating acute symptoms. Additionally, exploring the molecular mechanisms underlying MBT's neuroprotective actions is critical. Studies should investigate its effects on cholinergic signaling, acetylcholinesterase inhibition, oxidative stress mitigation, and modulation of pro-inflammatory pathways, such as the NF-$\kappa$B signaling cascade. Elucidating these mechanisms would clarify whether MBT acts through single or multiple neuroprotective pathways, a characteristic that could enhance its therapeutic relevance in a multifactorial disease like AD.

Safety evaluations must extend beyond acute toxicity to include subchronic and chronic toxicity testing (e.g., 28- or 90-day repeated-dose studies) accompanied by histopathological analysis of major organs, including the liver, kidneys, and brain, to establish a comprehensive safety profile. Advanced imaging and proteomic approaches such as cryo-electron microscopy, synaptosomal proteomics, and quantitative immunohistochemistry could provide deeper insight into MBT's role

in preserving synaptic integrity and neural architecture. Additionally, structure activity relationship (SAR) studies may facilitate the rational design of MBT analogs with improved potency, selectivity, and pharmacological properties.

On a translational level, exploring combination therapy paradigms involving MBT and established AD treatments (donepezil, memantine, or monoclonal antibodies like aducanumab) may reveal synergistic effects, particularly if MBT addresses complementary pathological pathways. The integration of biomarker discovery platforms, including plasma neurofilament light chain (NfL) and CSF cytokine panels, will enable the development of non-invasive tools to monitor treatment response and disease progression.

These strategies will collectively strengthen the preclinical foundation necessary to advance MBT toward clinical development for AD.

## 6.3 Limitations

While the study provides compelling evidence for the neuroprotective and anti-inflammatory efficacy of MBT in a scopolamine-induced AD model, several limitations constrain its interpretability and translational relevance. The acute scopolamine paradigm, though effective in modeling cholinergic dysfunction and transient cognitive deficits, fails to recapitulate the chronic, progressive neuropathology of AD, including amyloid-beta plaque deposition, tau hyperphosphorylation, and sustained neuroinflammation. Pharmacokinetic parameters, including bioavailability, blood-brain barrier permeability, and metabolic stability, remain uncharacterized, complicating dose optimization and clinical extrapolation.

# Bibliography

[1] R. N. L. Lamptey, B. Chaulagain, R. Trivedi, A. Gothwal, B. Layek, and J. Singh, "A review of the common neurodegenerative disorders: Current therapeutic approaches and the potential role of nanotherapeutics," *Int J Mol Sci*, vol. 23, no. 3, 2022.

[2] X. Zhao and D. L. Moore, "Neural stem cells: developmental mechanisms and disease modeling," *Cell Tissue Res*, vol. 371, no. 1, pp. 1–6, 2018.

[3] D. G. Gadhave, V. V. Sugandhi, S. K. Jha, S. N. Nangare, G. Gupta, S. K. Singh, K. Dua, H. Cho, P. M. Hansbro, and K. R. Paudel, "Neurodegenerative disorders: Mechanisms of degeneration and therapeutic approaches with their clinical relevance," *Ageing research reviews*, p. 102357, 2024.

[4] P. S. Aisen, G. A. Jimenez-Maggiora, M. S. Rafii, S. Walter, and R. Raman, "Early-stage alzheimer disease: getting trial-ready," *Nature Reviews Neurology*, vol. 18, no. 7, pp. 389–399, 2022.

[5] P. D. Emmady, C. Schoo, and P. Tadi, "Major neurocognitive disorder (dementia)," 2020.

[6] . A. disease facts and . h. figures. (2024). Alzheimer's & dementia : the journal of the Alzheimer's Association, 20(5).

[7] A. Kumar, J. Sidhu, F. Lui, and J. W. Tsao, *Alzheimer Disease*. Treasure Island (FL) ineligible companies. Disclosure: Jaskirat Sidhu declares no relevant financial relationships with ineligible companies. Disclosure: Forshing Lui declares no relevant financial relationships with ineligible companies. Disclosure: Jack Tsao declares no relevant financial relationships with ineligible

companies.: StatPearls Publishing Copyright © 2025, StatPearls Publishing LLC., 2025.

[8] D. Tromp, A. Dufour, S. Lithfous, T. Pebayle, and O. Després, "Episodic memory in normal aging and alzheimer disease: Insights from imaging and behavioral studies," *Ageing Res Rev*, vol. 24, no. Pt B, pp. 232–62, 2015.

[9] T. Ayodele, E. Rogaeva, J. T. Kurup, G. Beecham, and C. Reitz, "Early-onset alzheimer's disease: what is missing in research?" *Current neurology and neuroscience reports*, vol. 21, pp. 1–10, 2021.

[10] P. G. Ridge, M. T. Ebbert, and J. S. Kauwe, "Genetics of alzheimer's disease," *Biomed Res Int*, vol. 2013, p. 254954, 2013.

[11] S. P. Dickson, S. B. Hendrix, B. L. Brown, P. G. Ridge, J. Nicodemus-Johnson, M. L. Hardy, A. M. McKeany, S. B. Booth, R. R. Fortna, and J. S. K. Kauwe, "Genorisk: A polygenic risk score for alzheimer's disease," *Alzheimers Dement (N Y)*, vol. 7, no. 1, p. e12211, 2021.

[12] F. Khan and H. Qiu, "Amyloid-$\beta$: A potential mediator of aging-related vascular pathologies," *Vascular pharmacology*, vol. 152, p. 107213, 2023.

[13] X. H. Qian, X. X. Song, X. L. Liu, S. D. Chen, and H. D. Tang, "Inflammatory pathways in alzheimer's disease mediated by gut microbiota," *Ageing Res Rev*, vol. 68, p. 101317, 2021.

[14] R. H. Swerdlow and S. M. Khan, "The alzheimer's disease mitochondrial cascade hypothesis: An update," *Experimental Neurology*, vol. 218, no. 2, pp. 308–315, 2009. [Online]. Available: https://www.sciencedirect.com/science/article/pii/S001448860900017X

[15] S. Manoharan, G. J. Guillemin, R. S. Abiramasundari, M. M. Essa, M. Akbar, and M. D. Akbar, "The role of reactive oxygen species in the pathogenesis of alzheimer's disease, parkinson's disease, and huntington's disease: A mini review," *Oxid Med Cell Longev*, vol. 2016, p. 8590578, 2016.

[16] S. B. Kim, H. Y. Ryu, W. Nam, S. M. Lee, M. R. Jang, Y. G. Kwak, G. I. Kang, K. S. Song, and J. W. Lee, "The neuroprotective effects of dendropanax

morbifera water extract on scopolamine-induced memory impairment in mice," *Int J Mol Sci*, vol. 24, no. 22, 2023.

[17] S. H. Eason, N. R. Scalise, T. Berkowitz, G. B. Ramani, and S. C. Levine, "Widening the lens of family math engagement: A conceptual framework and systematic review," *Developmental Review*, vol. 66, p. 101046, 2022.

[18] J. Jack, C. R., J. S. Andrews, T. G. Beach, T. Buracchio, B. Dunn, A. Graf, O. Hansson, C. Ho, W. Jagust, E. McDade, J. L. Molinuevo, O. C. Okonkwo, L. Pani, M. S. Rafii, P. Scheltens, E. Siemers, H. M. Snyder, R. Sperling, C. E. Teunissen, and M. C. Carrillo, "Revised criteria for diagnosis and staging of alzheimer's disease: Alzheimer's association workgroup," *Alzheimers Dement*, vol. 20, no. 8, pp. 5143–5169, 2024.

[19] Z. Y. Chen and Y. Zhang, "Animal models of alzheimer's disease: Applications, evaluation, and perspectives," *Zool Res*, vol. 43, no. 6, pp. 1026–1040, 2022.

[20] O. Sheppard and M. Coleman, *Alzheimer's Disease: Etiology, Neuropathology and Pathogenesis*. Brisbane (AU): Exon Publications Copyright: The Authors., 2020.

[21] B. Opitz, "Memory function and the hippocampus," *Front Neurol Neurosci*, vol. 34, pp. 51–9, 2014.

[22] U. D. o. Health and H. Services, "What happens to the brain in alzheimer's disease," *National Institute on Aging*, 2017.

[23] Q. Deng, C. Wu, E. Parker, T. C. Liu, R. Duan, and L. Yang, "Microglia and astrocytes in alzheimer's disease: Significance and summary of recent advances," *Aging Dis*, vol. 15, no. 4, pp. 1537–1564, 2024.

[24] M. H. Mahnashi, M. Ashraf, A. H. Alhasaniah, H. Ullah, A. Zeb, M. Ghufran, S. Fahad, M. Ayaz, and M. Daglia, "Polyphenol-enriched desmodium elegans dc. ameliorate scopolamine-induced amnesia in animal model of alzheimer's disease: In vitro, in vivo and in silico approaches," *Biomed Pharmacother*, vol. 165, p. 115144, 2023.

[25] S. Srivastava, R. Ahmad, and S. K. Khare, "Alzheimer's disease and its treatment by different approaches: A review," *European Journal of Medicinal Chemistry*, vol. 216, p. 113320, 2021.

[26] E. Passeri, K. Elkhoury, M. Morsink, K. Broersen, M. Linder, A. Tamayol, C. Malaplate, F. T. Yen, and E. Arab-Tehrany, "Alzheimer's disease: Treatment strategies and their limitations," *Int J Mol Sci*, vol. 23, no. 22, 2022.

[27] I. Iqbal, F. Saqib, Z. Mubarak, M. F. Latif, M. Wahid, B. Nasir, H. Shahzad, J. Sharifi-Rad, and M. S. Mubarak, "Alzheimer's disease and drug delivery across the blood-brain barrier: approaches and challenges," *Eur J Med Res*, vol. 29, no. 1, p. 313, 2024.

[28] M. A. Azam and B. Suresh, "Biological activities of 2-mercaptobenzothiazole derivatives: a review," *Sci Pharm*, vol. 80, no. 4, pp. 789–823, 2012.

[29] F. Bermejo-Pareja and T. del Ser, "Controversial past, splendid present, unpredictable future: A brief review of alzheimer disease history," *Journal of Clinical Medicine*, vol. 13, no. 2, p. 536, 2024. [Online]. Available: https://www.mdpi.com/2077-0383/13/2/536

[30] A. E. Alkhalifa, N. F. Al-Ghraiybah, J. Odum, J. G. Shunnarah, N. Austin, and A. Kaddoumi, "Blood-brain barrier breakdown in alzheimer's disease: Mechanisms and targeted strategies," *Int J Mol Sci*, vol. 24, no. 22, 2023.

[31] V. Calsolaro and P. Edison, "Neuroinflammation in alzheimer's disease: Current evidence and future directions," *Alzheimers Dement*, vol. 12, no. 6, pp. 719–32, 2016.

[32] I. G. Onyango, G. V. Jauregui, M. Čarná, J. Bennett, J. P., and G. B. Stokin, "Neuroinflammation in alzheimer's disease," *Biomedicines*, vol. 9, no. 5, 2021.

[33] R. Dhapola, S. S. Hota, P. Sarma, A. Bhattacharyya, B. Medhi, and D. H. Reddy, "Recent advances in molecular pathways and therapeutic implications targeting neuroinflammation for alzheimer's disease," *Inflammopharmacology*, vol. 29, no. 6, pp. 1669–1681, 2021.

[34] M. Xu, L. Zhang, G. Liu, N. Jiang, W. Zhou, and Y. Zhang, "Pathological changes in alzheimer's disease analyzed using induced pluripotent stem cell-derived human microglia-like cells," *J Alzheimers Dis*, vol. 67, no. 1, pp. 357–368, 2019.

[35] D. R. Thal, M. E. Murray, and D. W. Dickson, *Alzheimer's disease (Aβ and Tau proteinopathy)*. CRC Press, 2024, pp. 1012–1041.

[36] S. Merighi, M. Nigro, A. Travagli, and S. Gessi, "Microglia and alzheimer's disease," *International journal of molecular sciences*, vol. 23, no. 21, p. 12990, 2022.

[37] P. Liu, Y. Wang, Y. Sun, and G. Peng, "Neuroinflammation as a potential therapeutic target in alzheimer's disease," *Clin Interv Aging*, vol. 17, pp. 665–674, 2022.

[38] D. V. Hansen, J. E. Hanson, and M. Sheng, "Microglia in alzheimer's disease," *Journal of Cell Biology*, vol. 217, no. 2, pp. 459–472, 2018.

[39] N. Torres-Acosta, J. H. O'Keefe, E. L. O'Keefe, R. Isaacson, and G. Small, "Therapeutic potential of tnf-$\alpha$ inhibition for alzheimer's disease prevention," *Journal of Alzheimer's Disease*, vol. 78, no. 2, pp. 619–626, 2020.

[40] C. Li, X. Zhang, Y. Wang, L. Cheng, C. Li, and Y. Xiang, "The role of il-1 family of cytokines in the pathogenesis and therapy of alzheimer's disease," *Inflammopharmacology*, vol. 32, no. 5, pp. 2681–2694, 2024.

[41] Z. Z. Si, C. J. Zou, X. Mei, X. F. Li, H. Luo, Y. Shen, J. Hu, X. X. Li, L. Wu, and Y. Liu, "Targeting neuroinflammation in alzheimer's disease: from mechanisms to clinical applications," *Neural Regen Res*, vol. 18, no. 4, pp. 708–715, 2023.

[42] J. M. Clarkson, J. E. Martin, and D. E. F. McKeegan, "A review of methods used to kill laboratory rodents: issues and opportunities," *Lab Anim*, vol. 56, no. 5, pp. 419–436, 2022.

[43] A.-K. Kraeuter, P. C. Guest, and Z. Sarnyai, "The y-maze for assessment of spatial working and reference memory in mice," *Pre-clinical models: Techniques and protocols*, pp. 105–111, 2019.

[44] J. Cortés-Ríos, A. M. Zárate, J. D. Figueroa, J. Medina, E. Fuentes-Lemus, M. Rodríguez-Fernández, M. Aliaga, and C. López-Alarcón, "Protein quantification by bicinchoninic acid (bca) assay follows complex kinetics and can be performed at short incubation times," *Analytical Biochemistry*, vol. 608, p. 113904, 2020.

[45] S. Saral, A. Topçu, M. Alkanat, T. Mercantepe, K. Akyıldız, L. Yıldız, L. Tümkaya, Z. A. Yazıcı, and A. Yılmaz, "Apelin-13 activates the hippocampal bdnf/trkb signaling pathway and suppresses neuroinflammation in male rats with cisplatin-induced cognitive dysfunction," *Behavioural brain research*, vol. 408, p. 113290, 2021.

[46] M. V Shreejha, R. Priyadharshini, P. Sinduja, and V. Meghashree, "Analysis of histological features of the cerebral cortex and hippocampus of albino rats using haematoxylin & eosin stain-an observational study," 2021.

# Appendices

## Appendix 1: Percentage spontaneous alternation in Y-maze (Day 1–6)

| Group | Day 1 | Day 2 | Day 3 | Day 4 | Day 5 | Day 6 | Mean ± SD |
|---|---|---|---|---|---|---|---|
| Control | 39.03 % | 35.50 % | 36.72 % | 37.31 % | 29.72 % | 33.40 % | 35.45 ± 3.24 % |
| Scopolamine(1 mg/kg) | 32.32 % | 37.90 % | 29.18 % | 23.37 % | 23.03 % | 19.82 % | 27.10 ± 6.86 % |
| Scop + Donepezil(5 mg/kg) | 21.13 % | 29.10 % | 26.71 % | 28.34 % | 25.19 % | 20.23 % | 25.78 ± 3.02 % |
| Scop + MBT(5 mg/kg) | 18.12 % | 24.85 % | 20.68 % | 22.03 % | 28.33 % | 24.50 % | 23.07 ± 3.59 % |
| Scop + MBT(10 mg/kg) | 20.33 % | 25.38 % | 23.22 % | 27.97 % | 28.33 % | 28.00 % | 25.37 ± 3.21 % |

## Appendix 2: Percentage spontaneous alternation in Probe test results (Day 7)

| Group | % Spontaneous alteration | | | | | | Mean ± SD |
|---|---|---|---|---|---|---|---|
| | 1 | 2 | 3 | 4 | 5 | 6 | |
| Control | 15.38 % | 22.00 % | 38.46 % | 30.76 % | 28.57 % | 30.00 % | 27.36 ± 8.00 % |
| Scopolamine(1 mg/kg) | 6.66 % | 8.30 % | 5.80 % | 20.00 % | 27.20 % | 25.00 % | 15.66 ± 9.19 % |
| Scop + Donepezil(5 mg/kg) | 25.00 % | 32.30 % | 21.00 % | 25.00 % | 26.30 % | 25.00 % | 25.10 ± 3.38 % |
| Scop + MBT(5 mg/kg) | 30.00 % | 20.00 % | 28.50 % | 30.00 % | 31.00 % | 35.00 % | 29.75 ± 5.45 % |
| Scop + MBT(10 mg/kg) | 25.00 % | 30.00 % | 30.00 % | 35.00 % | 35.00 % | 30.00 % | 30.83 ± 3.54 % |

# Appendix 3: Mean escape latency (seconds) from day 1 to day 6 in morris water maze test

| Day | Control group | Scopolamine (1mg/Kg) | Donepezil (5mg/kg) | MBT (5mg/Kg) | MBT (10mg/Kg) |
|---|---|---|---|---|---|
| **1** | 57.75 | 57.75 | 57.75 | 57.75 | 57.75 |
| **2** | 39.92 | 46.42 | 36.88 | 42.71 | 42.75 |
| **3** | 40.50 | 40.67 | 31.58 | 39.58 | 37.88 |
| **4** | 38.71 | 42.67 | 23.96 | 25.75 | 26.79 |
| **5** | 31.54 | 47.46 | 18.92 | 17.83 | 18.67 |
| **6** | 22.58 | 47.42 | 24.63 | 23.71 | 21.25 |

# Appendix 4: Mean time spent in target quadrant (seconds) on day 7 -Probe trial (MWM

| Group | Time spent (sec) | | | | | | Mean ± SD |
|---|---|---|---|---|---|---|---|
| | **1** | **2** | **3** | **4** | **5** | **6** | |
| **Control** | 15.38 | 22.00 | 38.46 | 30.76 | 28.57 | 30.00 | 27.20 ± 7.36 |
| **Scopolamine (1 mg/kg)** | 6.66 | 8.30 | 5.80 | 20.00 | 27.20 | 25.00 | 15.83 ± 9.12 |
| **Scop + Donepezil (5 mg/kg)** | 25.00 | 32.30 | 21.00 | 25.00 | 26.30 | 25.00 | 25.77 ± 3.28 |
| **Scop + MBT (5 mg/kg)** | 30.00 | 20.00 | 28.50 | 30.00 | 31.00 | 35.00 | 29.42 ± 4.62 |
| **Scop + MBT (10 mg/kg)** | 42.00 | 30.00 | 30.00 | 35.00 | 35.00 | 30.00 | 33.67 ± 4.50 |

# Appendix 5: Standard curve data for BCA assay

| Sr.no | Concentration ($\mu$g/mL) | Absorbance (OD) |
|---|---|---|
| 1 | 20 | 0.800 |
| 2 | 15 | 0.588 |
| 3 | 10 | 0.468 |
| 4 | 7.5 | 0.234 |
| 5 | 5 | 0.201 |
| 6 | 2.5 | 0.150 |
| 7 | 0 | 0.000 |

# Appendix 6: Sample group results for BCA assay

| **Groups** | **Mean Concentration ($\mu$g/mL)** |
|---|---|
| Control | 12.27 |
| Scopolamine (1 mg/kg) | 8.29 |
| Scop + Donepezil (5 mg/kg) | 11.66 |
| Scop + MBT (5 mg/kg) | 13.55 |
| Scop + MBT (10 mg/kg) | 15.57 |

# Appendix 7: Standard curve data for TNF-$\alpha$ expression measured by ELISA

| **Sr.no** | **Concentration ($\mu$g/mL)** | **Absorbance (OD)** |
|---|---|---|
| 1 | 90 | 2.532 |
| 2 | 60 | 1.721 |
| 3 | 30 | 0.981 |
| 4 | 15 | 0.701 |
| 5 | 7.5 | 0.407 |
| 6 | 0 | 0.055 |
| 7 | 90 | 2.532 |

# Appendix 8: Mean sample group results for TNF-$\alpha$ expression in mice hippocampus measured by ELISA

| **Sample Group** | **Mean Absorbance** | **Mean Concentration ($\mu$g/mL)** |
|---|---|---|
| Control | 0.449 | 10.6381 |
| Scopolamine (1 mg/kg) | 0.593 | 15.9532 |
| Scop + Donepezil (5 mg/kg) | 0.553 | 13.5328 |
| Scop + MBT (5 mg/kg) | 0.502 | 12.1755 |
| Scop + MBT (10 mg/kg) | 0.474 | 11.2137 |

# Appendix 9: Standard curve data for IL-1$\beta$ expression measured by ELISA

| Sr.no | Concentration ($\mu$g/mL) | Absorbance (OD) |
|---|---|---|
| 1 | 90 | 2.532 |
| 2 | 60 | 1.721 |
| 3 | 30 | 0.981 |
| 4 | 15 | 0.701 |
| 5 | 7.5 | 0.407 |
| 6 | 0 | 0.055 |

# Appendix 10: Mean sample group results for IL-1$\beta$ expression measured by ELISA

| Sample Group | Mean Absorbance | Mean Concentration ($\mu$g/mL) |
|---|---|---|
| Control | 0.449 | 10.6381 |
| Scopolamine (1 mg/kg) | 0.593 | 15.9532 |
| Scop + Donepezil (5 mg/kg) | 0.553 | 13.5328 |
| Scop + MBT (5 mg/kg) | 0.502 | 12.1755 |
| Scop + MBT (10 mg/kg) | 0.474 | 11.2137 |